REVIEW

Check for updates

Constructing strategies for hierarchically porous MOFs with different pore sizes and applications in adsorption and catalysis

Qizhao Xiong, Yang Chen, [ID] * Dongxiao Yang, Kaihua Wang, Yi Wang, Jiangfeng Yang, [ID] Libo Li [ID] * and Jinping Li [ID]

Since metal–organic frameworks, a versatile class of crystalline organic–inorganic hybrid materials featuring well-aligned intrinsic porosity, have come of age, the research focus has shifted from structural considerations toward the many fascinating properties enshrined in their real industrial applications. However, most MOFs reported to date only have microporous structures, which restrict mass transfer and inhibit macromolecules from accessing their pores. Hierarchically porous MOFs have been proposed because mesopores or macropores can alleviate these challenges. The strategies used to construct hierarchically porous MOFs have been discussed in this review article based on the pore size typically generated by each method and several instances of their applications in adsorption diffusion are shown. These applications demonstrate that the mass transport rate of hierarchically porous MOFs is improved when compared to pristine microporous MOFs, which is expected to solve the key problems found in application fields such as adsorption, catalysis, and sensing. Finally, the properties and challenges of hierarchically porous MOFs have been summarized, along with some recommendations for their future development.

1 Introduction

Metal–organic frameworks (MOFs) represent a new research direction combining coordination chemistry and materials science.[1,2] MOFs have developed rapidly and spawned a new class of porous materials after molecular sieves and porous organic polymers, which usually have the advantages of high porosity, low crystal density, and tunable pore size.[3] MOFs are porous materials formed *via* the self-assembly of metal nodes (or metal cluster) with organic ligands to develop a periodic porous framework. The self-assembly process strongly depends on the coordination preferences of the secondary structure units (SBUs) and the length and rigidity of the ligands used. In addition, it is affected by different reaction conditions, including the type of solvent, reaction temperature, reaction time, and ratio of metal ions to organic ligands.[4,5] The combination of different structural units allows this material to form functionalized porous surfaces as well as diverse structures. Therefore MOFs are considered ideal adsorbents for adsorption and separation.[6,7] Similarly, the wide range of potential applications of MOFs in gas storage,[8] photochemistry,[9] catalysis,[10] and sensing[11]

have also attracted extensive interest from researchers. Currently, more than 28 000 articles on MOFs have been recorded at the Cambridge Crystallographic Data Centre[12,13] and the research direction on MOFs has gradually developed from the construction of different structures to the possibility of their actual application.

International Union of Pure and Applied Chemistry (IUPAC) has defined pores with a pore size of <2 nm as micropores, pores in the range of 2–50 nm as mesopores, and pores >50 nm as macropores. In the field of gas separation, a proven strategy is to use micropores of pore sizes between the dynamic diameters of the gas molecules to sieve the gas mixture. However, in practical applications, the active sites of microporous porous materials are usually confined to the micropores, making the intrinsic mass transfer rates of microporous porous materials severely limited in catalytic and adsorption processes.[14] Despite the high selectivity of microporous MOFs for the separation of specific gas components, they are limited by slow mass transfer rates and low separation productivity. Thus, they have not been widely applied in industry.[15] To date, the majority of the reported MOFs are microporous and only a few MOFs materials have mesoporous or macroporous structures.[16,17]

The drawback that microporous MOFs restrict mass transfer and macromolecule passage can be solved by extending the chain length of the ligand to directly enlarge the pore size of MOFs. Therefore, the design and synthesis of long-chain

College of Chemical Engineering and Technology, Shanxi Key Laboratory of Gas Energy Efficient and Clean Utilization, Taiyuan University of Technology, Taiyuan 030024, China. E-mail: chenyangtyut@163.com, lilibo908@hotmail.com

organic ligands have been of great research interest, but the pore size has only been increased to 98 Å, which is probably the limit of what can be achieved by extending the ligand length.[18] Moreover, MOFs with extended ligand-constructed mesoporous structures usually collapse rapidly upon removal of the solvent because mesoporous topologies are more fragile than microporous structures. In addition, such extended ligand-constructed mesoporous MOFs are also prone to forming interpenetrating structures, leading to a significant reduction in the specific surface area and pore size. Therefore, the construction of hierarchically porous MOFs has been proposed to solve these problems. Two or more composite pore sizes in the same material is the key characteristic of hierarchically porous MOFs. When compared with conventional MOFs, the introduction of some larger pores can provide two or more pore advantages at the same time, such as the advantages of high specific surface area provided by micropores and the reduction of the molecular mass transfer resistance and accessible entrance of large molecules provided by mesopores and macropores.[19] As a result, hierarchically porous MOFs show great promise for various applications in the petrochemical industry.[20]

In most cases, the formation mechanisms of pores with similar sizes tend to have similarities during the formation of the hierarchical pores in MOFs. Therefore, the construction methods can be effectively classified according to the pore size formed by the hierarchical pores. In this paper, we introduce the methods used to construct hierarchically porous MOFs from micropores (mostly ligands with different functional groups are introduced), mesoporous (mostly pores formed by defects within the crystals), and macropores (predominantly pores formed by crystal stacking), and present the application advantages of hierarchically porous MOFs in adsorption and catalysis, as shown in Scheme 1.[21–28]

2 Constructing strategies at different pore scales

Extensive efforts have been made toward the construction of porous materials used for gas adsorption and separation, including hierarchically porous materials. For example, in our recent work, donut-like zeolite K-chabazite nanocrystal aggregates were obtained using a facile and green seed-passaging method, which exhibited a hierarchical macro–meso–microstructure.[29] The gas diffusion rate of this hierarchically porous material was significantly improved when compared to commercial adsorbents and exhibited the highest CH_4 adsorption capacity and separation performance recorded among commercial zeolites reported to date. Based on the characteristic that the pores of MOFs are more accessible to regulate than zeolites, it is expected that hierarchically porous MOFs will exhibit higher performance. Consequently, hierarchical porous MOFs with various mechanisms and their preparation methods are constantly emerging.[15,16,30–45] The current methods used to construct hierarchically porous MOFs usually have some drawbacks. For example, the template is easily repelled during the crystal growth process. In addition, it is difficult to control the pore size accurately in the strategies used to introduce defects, which usually results in the formation of a wide range of pore sizes. In addition, the etched pores are not uniform, which can easily cause pore blockage and the
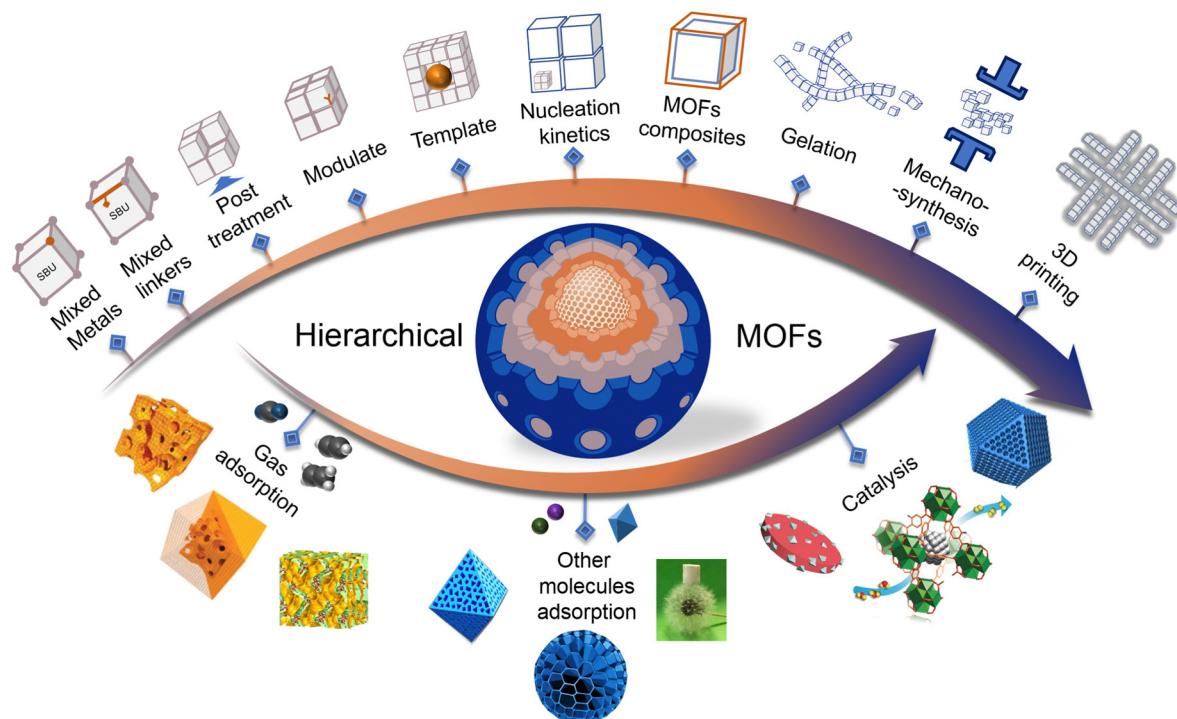
Scheme 1 Constructing strategies of hierarchically porous MOFs with different pore size ranges and their applications in adsorption and catalysis.[21–28]

introduction of impurities; the mixed ligand and MOF-on-MOF methods can only be used in a narrow range. Due to these drawbacks, these methods are generally not universal. To date, mesopores with relatively uniform pore size and adjustable range can be obtained using surfactants as templates. However, hierarchically porous materials simultaneously containing micropores, mesopores, and macropores have been rarely reported. Therefore, it is necessary to summarize the existing methods used to construct hierarchically porous and combine the advantages and disadvantages of the evaluation methods used for each application in order to obtain a general strategy for constructing hierarchically porous MOFs with adjustable pore diameters under relatively mild conditions.

2.1 Micropore scale

There are two main ways to construct MOFs with microporous–microporous hierarchical structures. One is the use of mixed metals and the other is to utilize mixed ligands (usually mixing the original ligands with derivatized ligands). The mass transfer rates of different molecules within MOFs are affected by the pore size, but also depend on the pore chemistry, therefore, appropriate ligands and metals can usually be selected to adjust the mass transfer rate of different molecules according to the type of functional groups present.[46]

2.1.1 Mixed metal strategy. There are usually two synthetic approaches used for the mixed-metal strategy: (1) metal exchange and (2) mixed-metal synthesis. The first approach involves direct synthesis from a mixture of the metal salts and MOFs. Mixed metals change the size of the original pores in the MOF. They can affect the adsorption and diffusion of different molecules or provide different active sites, and even improve the adsorption capacity. For example, Ti-exchanged UiO-66 exhibits an excellent CO_2 uptake capacity. After partial substitution of Zr^{4+} by Ti^{4+} in UiO-66, the CO_2 adsorption capacity at 273 K increases from 2.3 to 4 mmol g^{-1} (81 wt% improvement). When compared with pristine UiO-66, the exchanged UiO-66 (Ti/Zr) has a smaller pore size and stronger interaction between CO_2 and the Ti^{4+}-nodes, both of which are beneficial to improving the CO_2 adsorption capacity.[47] A schematic diagram of CO_2 adsorption by Ti-exchanged UiO-66 is shown in Fig. 1a.[48] The other approach is to introduce the second metal during the synthesis process. MOFs containing more than two metal ions mixed in one secondary structure unit are rare because the synthesis usually produces a mixed MOF phase rather than pure phases of the mixed metal MOF (MM-MOF). Wang *et al.* have directly synthesized MOF-74, which is capable of containing 10 different metals in pure phase crystals, as shown in Fig. 1b.[49] Controlling the spatial distribution of multiple metals in mixed-metal MOFs and the uniform distribution of mixed-metal secondary building blocks requires further understanding of the crystal formation mechanisms and interactions formed between the metals and ligands. When compared to the introduction of mixed metals during the synthesis process, metal exchange after synthesis is more likely to form a homogeneous phase.

2.1.2 Mixed ligand strategy. The mixed ligand strategy involves the introduction of active sites with different functional groups on the basis of the original MOF structure. Therefore, the pore size change is usually in the micropore range. Deng *et al.* introduced the first (MTV) MOF-5 with multiple ligands. Up to eight different ligands were simultaneously constructed in the MTV-MOF-5 materials (Fig. 1c).[50]
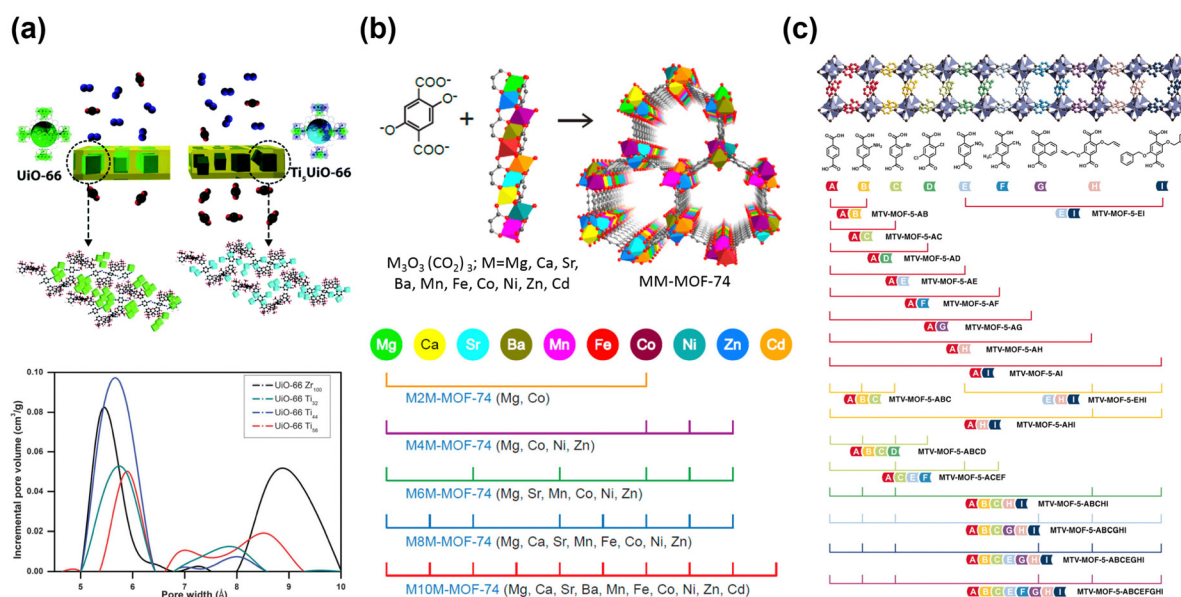
Fig. 1 (a) Ti-Exchanged UiO-66 enhances CO_2 adsorption capacity.[47,48] Reprinted with permission from ref. 48. Copyright 2013, The Royal Society of Chemistry. (b) Pure-phase MOF-74 crystals containing 10 different metals.[49] Reprinted with permission from ref. 49. Copyright 2014, American Chemical Society. (c) MTV-MOF-5 was constructed simultaneously with eight different ligands.[50] Reprinted with permission from ref. 50. Copyright 2010, American Association for the Advancement of Science.

BET analysis shows that the specific surface areas of MTV-MOF-EI and MTV-MOF-EHI are lower than that of MOF-5, but their CO_2 adsorption capacities significantly increase. In addition, mixed ligands lead to an increase in the CO_2/CO selectivity; the selectivity of MTV-MOF-EHI was improved by a factor of ~ 4, indicating that MTV-MOFs exhibit a substantial recognition of CO_2. Although the mixed ligand strategy has the advantages of pore size adjustment and functional group modification, there are still shortcomings in its application. The main problem is it is difficult control the structure constructed by the mixed ligands and the following two situations often occur: (1) the different ligands are unevenly distributed in the crystal and (2) the different ligands each grow into separate crystals.

In some cases, however, the pores introduced by the mixed ligands are mesopores as a result of a lack of ligands, mostly due to the different properties of the ligands used. For example, Jin *et al.* proposed a mixed ligand strategy to form hierarchically porous MIL-125 based on differences in the electronegativity.[51] Hierarchically porous MIL-125 with a series of continuously tunable mesoporous pore sizes can be obtained by simply adjusting the molar ratio of the two organic ligands, BDC-NH$_2$ (2-aminoterephthalic acid) and BDC (terephthalic acid). In addition, trimesic acid (btc) can be mixed with pyridine-3,5-dicarboxylate (pydc) to introduce structural defects to construct hierarchically porous Ru-MOF and reduce the valence of the Ru metal.[52] Mixed ligands can also be introduced under mild conditions utilizing a post-synthetic exchange (PSE) strategy,[53–55] which was named by Kim *et al.*[56] Cai *et al.* developed a general post-synthetic ligand substitution (PSLS) strategy to obtain more than 10 g of hierarchically porous UiO-66 and its composites

using a simple reflux system.[57] This strategy opens new doors for the fast, facile, versatile, and large-scale production of HP-MOF and its related composites to expand the application of conventional microporous MOF-based materials.

2.2 Mesopore scale

The principle of most methods used to construct mesoporous MOF is the formation of defects on an ordered network backbone, which is a simple and important method to obtain hierarchically porous MOFs. However, there are obvious disadvantages to this method, such as the difficulty to precisely control the pore size and the stability of the resulting structures. Structural stability not only refers to the overall structure of the MOF, but also refers to the mesoporous region after the formation of defects. The structural instability of the mesoporous region after the formation of defects causes part of the MOF structure to collapse, which cannot form uniform mesopores. There are several main strategies for defect construction, such as the post-treatment strategy, moderator strategy, and template strategy. In addition, conventional construction methods used to prepare mesoporous structures also include nucleation kinetics and MOFs composites.

2.2.1 Post-treatment strategy. The purpose of the post-treatment strategy is to form defective structures in order to construct mesopores. There are several main strategies used for defect construction, one of which is to controllably construct hierarchically porous MOFs using partially unstable ligands in mixed ligand systems under specific conditions. The process of constructing hierarchically porous MOFs using this method generally involves the initial synthesis of a pure phase MOF with both stable and unstable ligands. Defects are subsequently
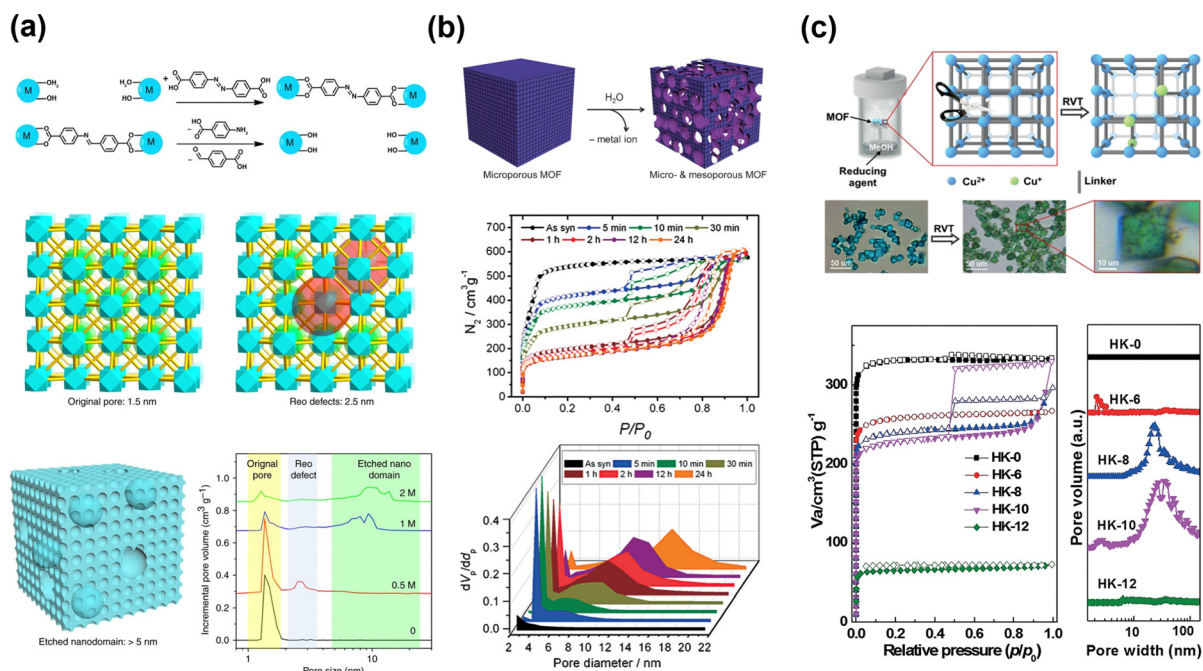

Fig. 2 (a) Schematic illustration of the process for obtaining hierarchically porous PCN-160 from chemically labile CBAB ligands.[58] (b) Schematic illustration of the post-synthesis hydrolysis to obtain the hierarchically porous POST-66(Y).[61] Reprinted with permission from ref. 61. Copyright 2015, Wiley. (c) The reduction of HKUST-1 by methanol steam formed hierarchically porous.[62] Reprinted with permission from ref. 62. Copyright 2019, Wiley.

formed to generate mesopores by removing the labile ligand. This method can controllably construct a hierarchically porous structure in a stable MOF. Hierarchically porous MOFs can be constructed using chemically unstable ligands. For example, Yuan et al. partially replaced the stable ligands in PCN-160 [Zr-AZDC] (AZDC = azobenzene-4,4′-dicarboxylate) with labile CBAB (4-carboxybenzylidene-4-aminobenzoate), followed by the hydrolysis of CBAB, which can achieve a controllable pore size from 1.5 to 18 nm, as shown in Fig. 2a.[58] The pore size of the resulting MOF can be controlled by two factors, the labile ligand content (i.e., the percentage of CBAB in PCN-160) and the concentration of acetic acid used during the hydrolysis step. Furthermore, hierarchically porous MOFs can also be constructed using thermally unstable ligands. Different from utilizing the chemical instability of the ligand, Feng et al. proposed a relatively general method, known as ligand pyrolysis, which can controllably generate mesopores in UiO-66-NH$_2$.[59] The ultra-small MO@HP-MOF composites (MO = ultra-small metal oxides) were formed via precise control of the decomposition temperature and exhibit stronger adsorption and catalytic performance. In addition, mesopores structures also can be constructed using another nine relatively thermally unstable ligands, indicating that this strategy is relatively versatile for the construction of UiO-66-based materials. The advantage of this method is that the crystallinity and the chemical stability of the MOF can be maintained after the ligand pyrolysis step generates the hierarchically porous structure. By controlling the pyrolysis temperature, heating time, and ratio of thermolabile ligands, the pore size can be tuned from 0.8 to 15 nm. However, the ligand-destabilized method requires the MOF to be highly stable.

Defect construction can also take advantage of the relative stability of MOFs. This method produces defects in a straightforward way by precisely dissolving a portion of the MOF crystals, forming mesopores with a pore size distribution that is typically broader than that of the mesopores formed using the ligand instability method. According to the different processing methods used,[60] most of these methods used to construct mesopores via etching the crystal can be divided into liquid-phase, gas-phase, and metal reduction (the principle is to reduce the coordination number of the metal, resulting in the absence of ligands and the formation of defects) methods. Liquid-phase etching methods include that reported by Kim et al., which obtained hierarchically porous POST-66(Y) via hydrolysis.[61] This method generates mesopores in the range of 3 to 20 nm in the MOF, which can be controlled by adjusting the time and temperature of hydrolysis, as shown in Fig. 2b. The resulting mesopore size increases upon increasing the dissolution time or temperature. Since the bridging ligands of some MOFs are carboxylic acid ligands, these MOFs are usually unstable under alkaline conditions. Etching these MOFs in alkaline solutions is likely to cause the rapid collapse of the MOF structure, so that the crystal can be etched with alkaline vapors under relatively mild conditions. For example, Albolkany et al. were the first to propose an ammonia etching strategy for HKUST-1, which can reversibly generate and repair mesopores with tunable pore size.[23] This strategy can generate

ordered mesopores on specific crystal planes of carboxylate-based microporous MOFs without affecting the crystal morphology. The pore sizes of the mesopores can be controlled by the etching temperature and the porosity of the mesopores can be adjusted by the pressure of etchant. The resulting mesopores can also be modified using the MOF precursor solution for controllable mesopore generation or encapsulation of the adsorbed molecules.

In addition, another method used to construct mesopores utilizing the crystal instability strategy is the metal reduction method. For example, Qi et al. reported an approach to construct hierarchically porous structures in HKUST-1 by tuning the valence state of the metal ions, as shown in Fig. 2c.[62] Their experiments showed that a portion of the Cu^{II} sites was reduced to Cu^{I} by the CH$_3$OH vapor, which destroys some of the coordination bonds, resulting in the formation of mesopores in the microporous framework and the formation of macropores. Moreover, Song et al. used hydroquinone (H$_2$Q) to reduce Cu^{2+} ions in HKUST-1 for the first time to obtain mesopores.[63] Using single-crystal X-ray diffraction, CO adsorption, and ^{1}H NMR spectroscopic analysis, it was demonstrated that the treatment of HKUST-1 with H$_2$Q under anhydrous conditions resulted in the reduction of 33.3% of the Cu^{2+} sites (half of the framework Cu$^+$ and half of the free Cu$^+$ sites). The reduction reaction will not proceed any further once 33.3% of the Cu^{2+} sites are reduced to Cu$^+$. This phenomenon is due to the fact that HKUST-1 has a limited number of pore cages. Furthermore, coordination reduction results in a significant enhancement of the hydrolytic stability of HKUST-1, which remains structurally intact even after two years of exposure to humid air.

2.2.2 Modulator strategy. The modulator strategy usually involves co-assembly with monocarboxylic acids to controllably create defects. Liu et al. used a low-dose HRTEM technique to study the defects of formic acid regulators constructed in UiO-66 during the synthesis process via direct imaging and some of the images are shown in Fig. 3a.[64] It was found that ligand defects predominate, while cluster defects only appear in small regions; as the crystal grows, only the ligand-lacking defects remain. The defect evolution can be reversed by increasing the concentration of the regulator (formic acid). These observations provide insight into the evolution of MOF defects, including their types and distributions. Kim et al. first proposed an acetic acid co-assembly strategy to generate mesopores in HKUST-1.[65] This hierarchically porous HKUST-1 material exhibits a higher methane adsorption capacity (13% higher storage capacity at 65 bar) and significantly increased surface area (from 1787 to 2396 m^2 g^{-1}) when compared to the original HKUST-1. Carboxylic acids coordinate with the metal ions to form metal-oxygen clusters. At the same time, the alkyl chains create structural defects and additional pore space, so the pore size can be systematically tuned by varying the length and concentration of the modulators used. Kirchon et al. obtained PCN-250 with tunable mesopore pore sizes using fatty acids with different alkyl chain lengths and concentrations as the regulator, as shown in Fig. 3b.[66] Similarly, Cai et al. used a monocarboxylic acid as the modulator to prepare hierarchically porous MOFs,
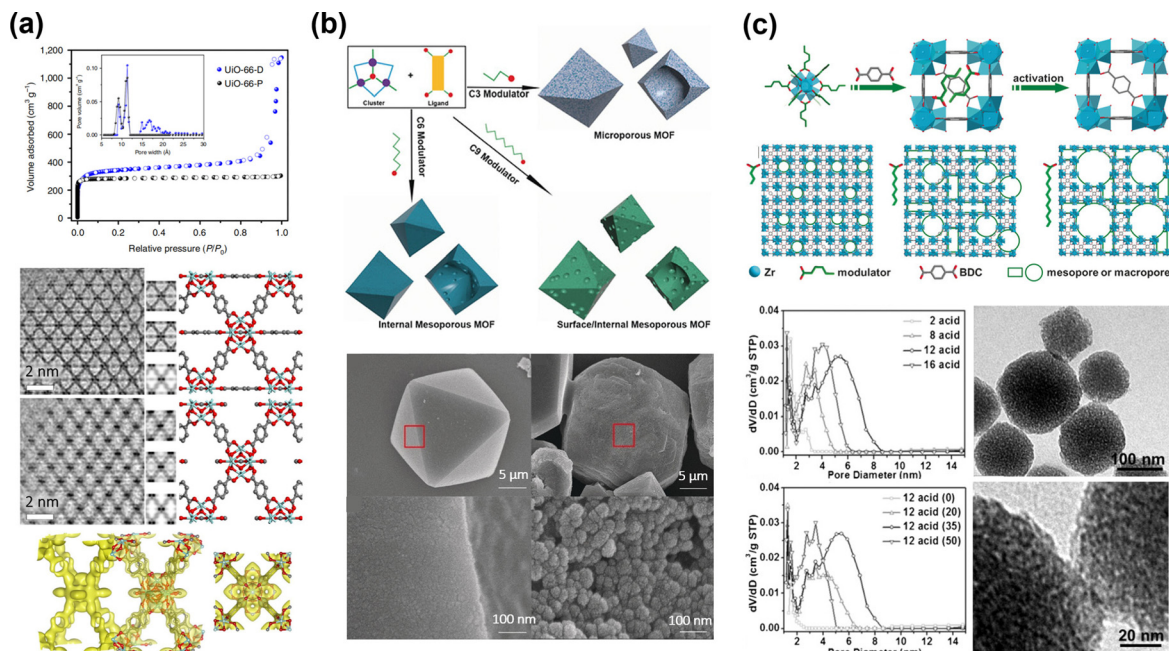
Fig. 3 (a) HRTEM analysis of missing ligands in UiO-66.[64] Reprinted with permission from ref. 64. Copyright 2019, Nature Publishing Group. (b) Schematic diagram of the preparation of hierarchically porous PCN-250 with monocarboxylic acid as modulator.[66] Reprinted with permission from ref. 66. Copyright 2019, Wiley. (c) The pore size of mesoporous UiO-66 is systematically adjusted by changing the concentration of acetic acid.[67] Reprinted with permission from ref. 67. Copyright 2017, Wiley.

including UiO-66 and its derivatives, MIL-53, DUT-5, and MOF-808, as shown in Fig. 3c.[67] Other works using acetic acid as a modulator to construct hierarchically porous MOFs have been reported, such as Ma *et al.* study on UiO-66-NH$_2$ with tunable mesopores They systematically investigated the effect of this structural defect on photocatalysis.[27] Other modulators can be used to construct hierarchically porous MOFs. For example, Liu *et al.* synthesized hierarchically porous HKUST-1 under hydrothermal synthesis conditions using a simple one-step mixing of trimesic acid and benzoic acid.[68] Using benzoic acid as the modifier to partially replace the trimesic acid ligands, the paddlewheel structure was twisted to adapt to its coordination and in addition to the original micropores in HKUST-1, meso-pores were generated in this twisted structure. Wang *et al.* used trifluoroacetic acid (TFA) as a modifier to construct defects in UiO-66 to form a hierarchically porous MOF and a number and types of the structural defects in UiO-66 (*i.e.*, missing cluster defects or missing ligand defects) could be regulated by precise control of synthesis or processing conditions. Both types of structural defects can increase the number of effective open metal sites.[69] The greatest advantage of the modulator strategy is that it can usually form two pore sizes of mesopores, but there are still some problems to be solved. First, adjusting the molar ratio of the modulator cannot precisely adjust the pore size of the pores formed by the defects. Secondly, the addition of monocarboxylic acids will affect the formation of MOFs, especially MOFs bearing imidazole ligands. Consequently, it is still necessary to solve how MOFs from the same reaction precursors with different topologies can be used to construct other building units using the regulator strategy. The key to

fabricating defects in this way is choosing the suitable modifier.

2.2.3 Template strategy. Another common strategy to intro-duce defects in MOFs is to use templating agents (such as surfactants and hard templates). Methods that require the formation of the template under the reaction conditions (such as the presence of a surfactant) are known as soft-templating methods. In contrast, the hard-template method involves the template to be formed prior to beginning the reaction. The soft-template method has been widely favored due to its relatively ubiquitous and tunable pore structure. The soft-template method has two main prerequisites, the surfactant must form stable micelles in the solution and the surfactant must form a strong interaction with the MOF precursor. However, since the synthetic solution used for the preparation of MOFs is composed of organic solvents with amphiphilic properties, it is difficult for most surfactants to form stable micelles. There are only a few ionic surfactants or amphoteric blocks used for the preparation of hierarchically porous MOFs. Qiu *et al.* reported the preparation of micro–mesoporous HKUST-1(Cu$_3$(BTC)$_2$(H$_2$O)$_3$), which was the first example of the construction of a hierarchically porous MOF using the soft template method.[70] CTAB (cetyltri-methylammonium bromide) was added to the MOF precursor solution in the solvothermal synthesis used to obtain hierarchi-cally porous HKUST-1, in which the molar ratio of CTAB and Cu^{2+} could be adjusted to increase the specific surface area and volume of the mesopores, and the maximum pore size was 5.6 nm. The hydrophobic TMB surfactant was used in conjunction with CTAB to further expand the mesopores and the maximum mesopore pore size could be extended to 31 nm. MIL-100 can also be

synthesized using CTAB to build hierarchically porous structures.[71] This showed that in the presence of CTAB, changing the pH and molar ratio of H_2O to EtOH in the synthesis will affect the micelle configuration and ligand solubility, resulting in three different topologies: MIL-96, MIL-100, and MIL-110. Controlling the pH, the molar ratio of the surfactant to metal, and molar ratio of the solvent (H_2O to EtOH) can be used to tune the pore size of the mesopores between 3 and 33 nm. However, the template is often repelled due to the weak interaction formed between the template and the precursors, allowing the independent nucleation of the MOFs during the crystal growth process. Thus, the interactions formed between the metal ions and surfactant molecules can be enhanced using citric acid.[72] The resulting hierarchically porous HKUST-1 formed 20 nm mesopores. They proposed a general co-assembly mechanism, in which the inorganic salts combine with the surfactant molecules to form intermediates.[73] A study has used a dicationic quaternary ammonium as a soft templating agent utilizing weak electrostatic interactions to obtain hierarchically porous Cu-BTC.[74] 1,3,5-Trimethylbenzene can be used to expand the pore size of the mesopores with dicationic quaternary ammonium *via* their synergistic effects. Recently, Yang *et al.* constructed regular macroporous channels up to 100 nm and uniform macroporous walls of 11–12 nm in UiO-66(Ce) by systematically adjusting the feed ratio of P123/F127 and the amount of toluene used, as shown in Fig. 4a.[24] When compared with the generation of defects or the use of long alkyl chain ligands, the hierarchically porous MOFs constructed using the soft templating method can precisely tune the porosity to form mesopores with uniform pore sizes. The mesopores introduced using the soft templating method typically depend on the size of the micelles formed by the surfactant.

MOFs can also encapsulate nanoparticles with the desired size and then etch the encapsulated particles to form hierarchically porous materials. The encapsulated particles need to have functional groups that can interact with the MOF precursors. For example, Shen *et al.* used highly ordered polystyrene microspheres (PS) as the hard template and ZIF-8 as the research object. They reported the world's first ordered macroporous–microporous MOF in the form of a single crystal, as shown in Fig. 4b. This opened up the field of three-dimensional ordered macroporous–microporous materials.[28] The ZIF-8 precursor was assembled and grown on the highly ordered monodisperse PS nanospheres. Finally, the PS template was removed using THF selective etching to obtain the highly ordered macroporous–microporous ZIF-8 single crystals. The size of the hard template determined the pore size of the mesopores. However, hard templates are sometimes tricky to remove without destroying the crystallinity of the MOF. Therefore, another approach to the hard template method has been developed, which is to use the reactant as the template (usually a metal or ligand source that is insoluble in the solution), and the formed MOF nanoparticles are stacked and grown around the template. Therefore, the template is involved in the reaction. The mesopores formed using the self-sacrificial template method are constructed *via* the self-sacrificial formation of defects. Therefore, the pore size formed using this method also depends on the size of the template used, but it is not controllable when compared with the soft template method and other hard template methods. Zhang reported a simple and effective self-sacrificial templating strategy based on the nanoscale Kirkendall effect to form hollow nanorod structures of Co-MOF-74, which can efficiently adsorb/desorb gas molecules.
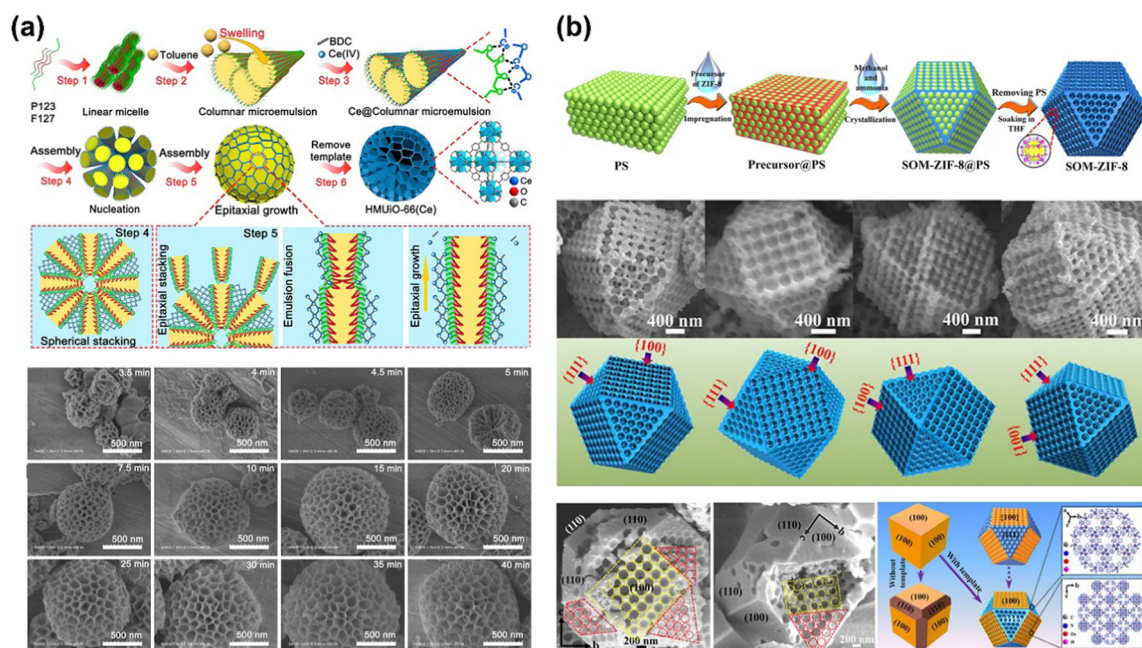

Fig. 4 (a) Construction of hierarchically porous UiO-66(Ce) by soft template method.[24] Reprinted with permission from ref. 24. Copyright 2022, American Chemical Society. (b) Using highly ordered PS to construct hierarchically porous ZIF-8.[28] Reprinted with permission from ref. 28. Copyright 2018, American Association for the Advancement of Science.

This nanostructured MOF-74 shortens the diffusion distance and increases the rate of CO_2 gas adsorption under dynamic adsorption conditions.[75] In addition, ionic liquids, CO_2-expanded liquid, *etc.* can also be used as templates to construct hierarchical porous MOFs.[76,77]

2.2.4 Nucleation kinetics. In addition to the methods mentioned beforehand used to construct mesopores, nucleation kinetics is a more straightforward method to make the MOF crystals stack during the crystal growth process to form mesoporous by controlling several conditions for crystal nucleation during the reaction. Yue *et al.* reported a rapid template-free synthesis of hierarchically porous Zn-MOF-74 at room temperature.[78] The morphology of the hierarchically porous Zn-MOF-74 increases with the reaction time, from the surface formed by large crystallites to the surface formed by the accumulation of nanoparticles. The reaction solvent can also be changed to control the crystallinity and adsorption properties of hierarchically porous Zn-MOF-74. The pore size of Zn-MOF-74/0.25 obtained after 15 min of reaction was 9 nm, and after 10 d of reaction this was ~15 nm. Besides adjusting the reaction time, the crystal nucleation can also be influenced by adjusting the reaction temperature, thereby constructing hierarchically porous MOFs. Cao *et al.* controlled the pores formed by the packing of nano-HKUST-1 particles under solvothermal conditions by simply changing the synthesis temperature, resulting in mesopores with pore sizes ranging from 26 to 72 nm.[79] When the reaction temperature was low, small nanoparticles are formed, and when the reaction temperature is high, the nanoparticles formed become larger, and larger mesopores are formed by their loose packing. Therefore, with the increase in the reaction temperature, the average pore size of the mesopores increases. Moreover, this method of constructing mesopores can be applied in other organic solvents, such as methanol, *n*-propanol, DMF, *etc.* The solvent of the reaction system can also be adjusted, for example, Li *et al.* developed a hierarchically porous material comprised of UiO-66(Hf) and other UiO-66-based MOFs by adjusting the molar ratio of monocarboxylic acid/water. The mesoporous pore size can be adjusted in the range from 3 to 13 nm, as shown in Fig. 5a.[80] As the amount of H_2O increases, the crystal size decreases, and thus, the mesopore size decreases. These experiments show that mesopores are beneficial to the adsorption and catalysis of macromolecules.

2.2.5 MOF composites. MOFs can also be composited with porous materials with different pore sizes (including MOFs, porous organic polymers, and carbon materials). The obtained porous composites can contain the features of both materials, which can be widely used in different applications. The composite of MOFs with other MOFs can form porous materials with both characteristics of the MOFs and two kinds of pores, and even realize the possibility of one-step separation and purification or one-step catalysis.[81] MOFs composites exhibit different pore sizes depending on the materials used. MOF-on-MOF also form mesopores. For example, Zhao *et al.* showed that PCN-222 (also known as MOF-545) nanorods can be selectively grown along both ends of the long ellipsoid axis of PCN-608 nanocrystals and NU-1000 hexagonal prism-like structures can be formed along the two basal planes of the nanorod crystals and the upper and lower basal planes of PCN-134
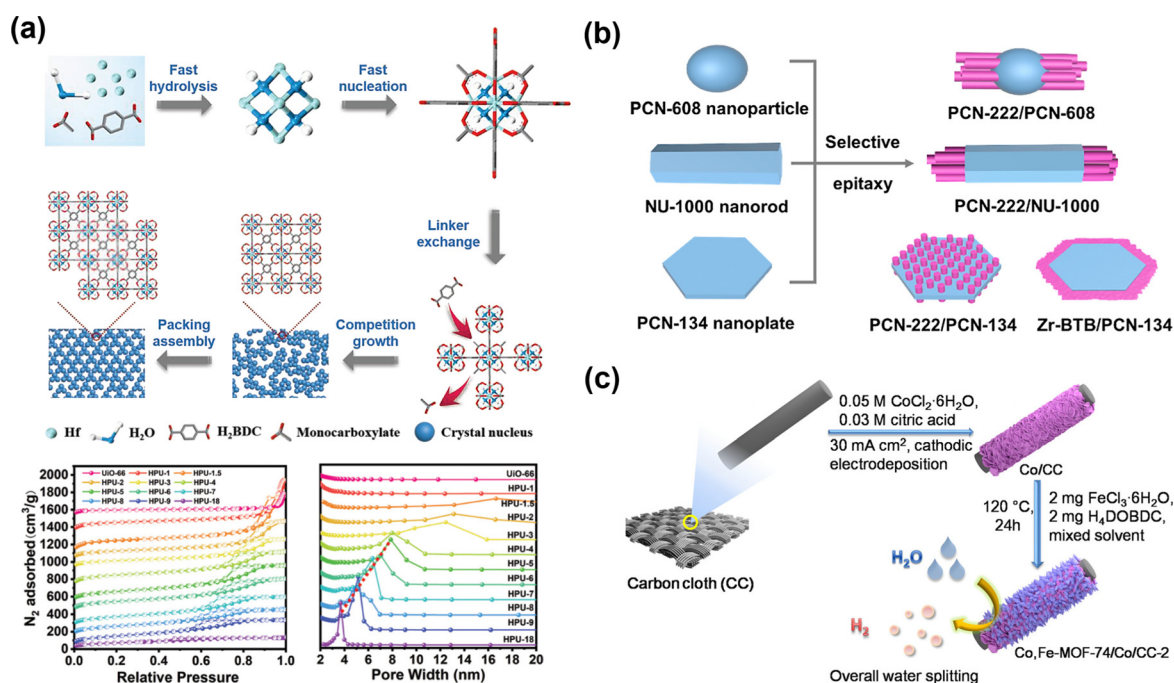
Fig. 5 (a) Nearly linear adjustment of the mesopore pore size of hierarchically porous UiO-66(Hf) by adjusting the molar ratio of monocarboxylic acid/water.[80] Reprinted with permission from ref. 80. Copyright 2021, Wiley. (b) Selectively grown to form hierarchical structure MOFs.[82] Reprinted with permission from ref. 82. Copyright 2020, American Chemical Society. (c) MOF-74 arrays are closely arranged on the surface of Co/CC rods.[85] Reprinted with permission from ref. 85. Copyright 2020, American Chemical Society.

hexagonal nanosheets. The Zr-BTB nanosheets selectively grow on the sides and six edges surface of the PCN-134 hexagonal nanosheets. A schematic illustration of the selective growth of MOFs to form a layered structure is shown in Fig. 5b.[82] The MOF-on-MOF strategy usually requires the structure to be identical to the composite material rather than separate phases. Zhuang et al. used the same approach to synthesize composite materials with different crystal structures and chemical properties.[83] A layer of mesoporous silica was wrapped on UiO-66@ZIF-8 mediated by CTAB, forming a stable core–shell–shell hierarchical nanoporous material. The main role of CTAB was to reduce the high interfacial energy caused by the topological mismatch between the core–shell components.

There are also methods of compounding MOFs with other porous materials, such as mixed matrix membranes. At the same time, there are problems such as the incompatibility between the MOFs and polymer, and clogging of the pores. Wang et al. reported the conversion of an MOF-on-MOF to MOF–polymer composite. This templated synthesis allows the introduction of MOFs of various sizes, distributions, and concentrations into polymeric matrices, which partially form mesopores.[84] In the work of Zha et al., a hierarchically structured Co, Fe-MOF-74/Co/CC (carbon layer) hybrid electrode nanorod structure was obtained using a simple solvothermal treatment method.[85] MOF-74 arrays are densely arranged on the surface of Co/CC rods, forming a hierarchical structure, as shown in Fig. 5c. McDonald et al. uniformly grafted PMMA (polymethyl methacrylate) on a core–shell MOF, IRMOF-3@MOF-5, maintaining its internal porosity.[86] Since the PMMA polymerization initiator can be bound to the amino group using a post-synthesis modification method, the thickness of the polymer film can be controlled by adjusting the thickness of the shell layer carrying the initiator. This strategy to form MOF composites usually enables the materials to exhibit better properties than single pure-phase MOFs. However, the synthesis conditions are relatively harsh, which not only imposes certain restrictions on the MOFs used, but the stability of the MOFs is also required in some cases. In general, this strategy is easier to nucleate on its own than to form composites. Of course, the most considerable difficulty faced by such composite MOF materials with mismatched topologies is how to solve the high interface energy as a result of mismatched topologies.[87] To rise above the energy barrier, the use of surfactants or structure-directing agents is an option to simultaneously grow two different MOFs, especially with different topological structures. Otherwise, the crystal growth behaviors need to be adjusted to overcome the surface energy.[88]

2.3 Macropore scale

The macropores introduced in the MOF are usually formed by the accumulation of MOF crystals and the methods used to develop macropores by introducing defects are generally difficult because of their tendency to cause structural instability in the MOF. The main techniques of MOFs crystal accumulation to form macropores include MOF gelation, mechanical synthesis, and 3D printing.

2.3.1 Gelation of MOFs. On the macroporous scale, MOF nanoparticles can stack to form intergranular macropores using gelation methods. The gelation method combines rigid frames into flexible gels in various solvents. Lohe et al. reported the rapid synthesis of MIL-100(Fe) aerogels with internal micropores and macroporosity at room temperature.[89] The samples showed a wide pore size distribution from micropores to mesopores, and even macropores without long-range ordering. Xiang et al. explored the gel synthesis of Fe^{3+} and Cr^{3+} metal ions with various carboxylic acid ligands, while delving into the gelation process.[90] Highly porous aerogels can be prepared from rigid carboxylate ligands, such as BDC and BTC. Aerogels have tunable porous structures with micropores and mesopores that can be adjusted by the reactant concentration. At high reactant concentrations, Cr-BTC materials are predominantly microporous, in contrast to hierarchical structures with narrow mesopore size distributions at lower concentrations. Li et al. further proposed a general and facile synthesis route for the two-step gelation of ultralight hierarchically porous MOFs aerogels to synthesize hierarchically porous MIL-53 nanoparticles with various ligands, as shown in Fig. 6a.[22] The first step of the gelation process is the formation of MOF clusters and the second step is the breaking of the ligand equilibrium. The critical factor for inducing the sol–gel transition is the selection of a suitable gel temperature. The pore sizes can be adjusted from 3.6 to 87.8 nm by controlling the concentration or temperature. The temperature causes the MOF crystals to transform into non-crystalline nanoparticles so that the crystals no longer grow and cross-link with each other. The mesopore size of the aerogels can be manipulated by changing the concentration of the reactants and the mediating effect of surfactants. The gelation method can obtain hierarchically porous MOF gels with tunable porosity, high surface area, and low density. However, the disadvantage is that the original crystallinity and micropores of the MOF are usually sacrificed.

2.3.2 Mechanosynthesis of MOFs. Mechanosynthesis is an efficient and environmentally friendly alternative method for synthesizing MOFs. The MOFs obtained via mechanosynthesis usually have hierarchically porous structures, which have good applications in the adsorption of macromolecules and catalysis.[91] Currently, mechanosynthesis allows the preparation of various MOFs, such as MOF-5,[92] HKUST-1,[93] MIL-101,[94] UiO-66[95] and the ZIF series of MOFs.[96,97] These MOFs obtained by mechanical synthesis usually have high specific surface areas, which are not lower than MOFs prepared using conventional solvothermal methods.[98] For example, Yang et al. used NaCl or KCl as a solid solvent and template to assist the mechanical synthesis of HKUST-1 with microporous, mesoporous, and even macroporous structures, as shown in Fig. 6b.[99] By adjusting the amounts of NaCl and TED added, the type of mesopores, proportion of pores, pore size, and number of functional groups can be controlled. Moreover, the MOFs synthesized using salt-assisted mechanochemistry exhibit higher performance in trapping iodine vapor than the products prepared via heating in solvent. Furthermore, Tanaka et al. proposed a mechanosynthetic method in which ZIF-8 could be obtained via
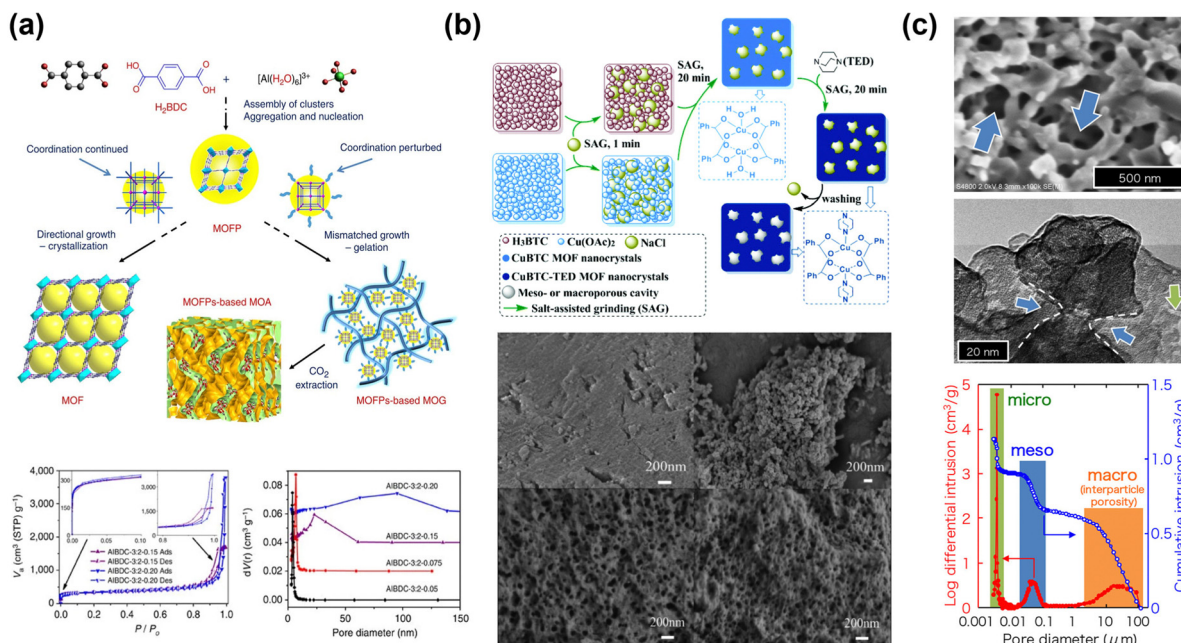
Fig. 6 (a) Schematic representation of MIL–53 (Al) gel formation.[22] (b) Mechanical synthesis of HKUST-1.[99] Reprinted with permission from ref. 99. Copyright 2018, The Royal Society of Chemistry. (c) Mechanical synthesis of ZIF–8.[100] Reprinted with permission from ref. 100. Copyright 2017, American Chemical Society.

the rapid reaction of ZnO and 2-methylimidazole under solvent-free conditions using zinc acetate dihydrate as a partial Zn source and catalyst, as shown in Fig. 6c.[100] The adsorption capacity of rhodamine B by mechanically synthesized ZIF-8 (9.6 μmol g^{-1}) was much higher than single crystal ZIF-8 (2.9 μmol g^{-1}) because of the macroporous structure formed by the accumulation of nano-ZIF-8. Under solvent-free conditions, it is safer and more environmentally friendly to use metal oxides instead of metal salts. For example, Julien *et al.* demonstrated the real-time *in situ* monitoring of Zn-MOF-74 prepared *via* mechanosynthesis on a gram-scale. They revealed two new intermediate phases of ZnO during the direct mechanosynthesis of Zn-MOF-74, as well as an unusual stepwise reaction mechanism in which the tightly packed intermediates react to form an open framework.[101] The presence of a small amount of solvent in the mechanochemical synthesis process enhances the mobility of the metal ions and organic ligands, thus facilitating the chemical reaction and improving the reaction rate and crystallinity of the product.[102] For example, water in the grinding solution accelerates the mechanosynthesis process and the BET surface area of Zn-MOF-74 obtained from the synthesis with DMF in the grinding solution matched the highest value reported to date.[103] The hierarchical pore structure was formed according to type II and type IV isotherms. Furthermore, ultrasonic synthesis provides MOF crystals with smaller size.[104] Abbasi *et al.* reported the ultrasonic synthesis of hierarchically porous nano-HKUST-1 (U-CuBTC) and compared the adsorption and release capacity of crystalline violet (CV) and methylene blue (MB) with HKUST-1 (M-CuBTC) obtained *via* mechanical synthesis.[105] When compared to M-CuBTC, U-CuBTC has a lower specific surface area and larger average

mesopore pore size. Upon comparison, the adsorption capacity of U-CuBTC for MB (33.7%) and CV (27.5%) significantly exceed that of M-CuBTC for MB (22.9%) and CV (11.9%).

2.3.3 3D printing. Thakkar *et al.* reported the use of 3D printing technology to fabricate post-molding MOFs for the first time and investigated their CO_2 adsorption properties.[106] In this study, pre-prepared MOF powder and bentonite (as a binder) were mixed in ethanol. The resulting mixture was added to a mixture of polyvinyl alcohol (PVA) and deionized water to form an extrudable paste, which was then loaded into a 3D printer to produce macroscopically shape-tunable MOF monoliths, as shown in Fig. 7a. MOF-74(Ni) and UTSA-16(Co) monoliths with MOF loadings of up to 80 and 85 wt%, respectively, were fabricated by 3D printing, preserving the physical properties and complete structure of the pristine MOF powders. In addition, when comparing the penetration test of UTSA-16(Co) monolith and powder, the UTSA-16(Co) monolith reached the adsorption equilibrium faster, indicating faster adsorption kinetics than its corresponding powder form. When compared with other methods used to fabricate microporous MOFs, 3D printing can efficiently synthesize MOFs with multiple complex structures and easily reproducible experiments.[107] In addition, the preparation of MOF composites is easier than conventional MOFs that requires the bonding of ligands with specific functional groups, and 3D printing makes it easier to form MOFs with additional macroporous when compared to the conventional solvent thermal synthesis.[108] For example, a ZIF-67 monolith with a macrostructure has been synthesized using 3D printing, as shown in Fig. 7b.[109] Current technology for 3D printing MOFs focuses on the fabrication of molded MOFs monoliths with the ability to introduce hierarchical structures.[110] However, the current
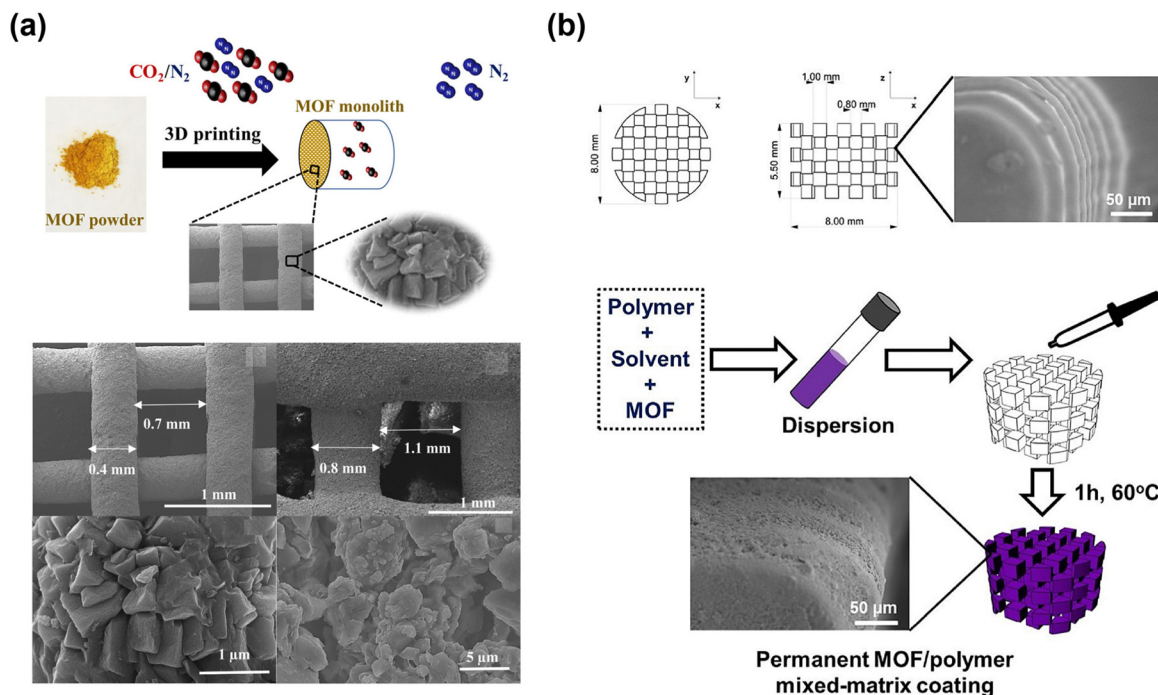
Fig. 7 (a) Schematic diagram of the 3D printed synthetic MOF monolith.[106] Reprinted with permission from ref. 106. Copyright 2017, American Chemical Society. (b) 3D printing synthetic ZIF–67 monolith.[109] Reprinted with permission from ref. 109. Copyright 2019, Elsevier.

technology for 3D printing MOFs may be immature and most of the micropores in the MOFs will be lost in most cases.[111] In addition, 3D printing may not be suitable for synthesizing MOFs that are unstable in the air because the layer-by-layer printing process may require prolonged exposure to air (15–120 h).[112] When 3D printing technology becomes more mature, the structure and pore sizes of MOFs will be tailored more precisely.

3 Hierarchically porous MOFs used for adsorption and catalysis

3.1 Gas adsorption

The purpose of constructing hierarchically porous MOFs *via* various methods is to meet the multiple needs of their practical applications, such as their widespread use to address slow diffusion in gas adsorption.[20] The pore size distribution usually enhances the gas adsorption and mass transfer rate of hierarchically porous MOFs and therefore, they are widely used in gas adsorption.[113] CO_2, a major greenhouse gas, is a major industrial gas that contributes to climate change and global warming. Therefore, it is of great importance for human development to study the removal of CO_2.[114–117] The selective adsorption of CO_2, CH_4,[118–120] and H_2[121–123] using mesoporous MOFs indicates that mesopores have a high gas adsorption capacity. In addition, hierarchically porous MOFs can also modulate the shape of the pores or modulate the selective adsorption of different molecules.[32] The improved performance of hierarchically porous MOF materials in gas adsorption compared to pristine MOFs can be presented as an

example of CO_2 adsorption. This is due to the presence of more channels in the hierarchically porous MOF crystals, which increases the specific surface area and molecular diffusion mass transfer rate, increasing the CO_2 gas loading rate.[124]

A mixed-ligand strategy has been used to construct a hierarchically porous MOF capable of enhancing CO_2 adsorption, which can introduce functional groups that have an effect on CO_2 or expose uncoordinated carboxylic acid groups. For example, Park *et al.* co-assembled TPTC (terphenyl-tetra carboxylate) and R-isoph (5-R isophthalic acid, R represents a functional group) to introduce functionalized mesopores in PCN-125.[125] The introduced functional groups enhance the interaction with CO_2 and most of the R(N)-PCN-125 materials exhibit higher CO_2 uptake and heat of adsorption when compared to pristine PCN-125, although the specific surface area is lower, and NH_2(1)-PCN-125 has a higher CO_2 uptake at 130 mmHg than pristine PCN-125. The CO_2 uptake of NH_2(1)-PCN-125 was 30% higher than that of pristine PCN-125, as shown in Fig. 8a. The functionalized MOF obtained using this strategy has a better effect on CO_2 adsorption when compared with conventional surface modification methods.

Introducing defects into MOFs generally improves their ability to adsorb CO_2. For example, Wu *et al.* reported a general gas matching exchange (VPLE) method for the post-synthesis modification of MOFs.[126] Using VPLE, ligands with functional groups can be inserted into MOF *via* ligand exchange. VPLE also allows multi-stage operations to obtain MOF materials with multiple ligands and functional groups. Among them, ZIF-8/Br exhibits a high CO_2/N_2 adsorption selectivity of 31.1 and CH_4/N_2 of 10.8, which are higher than the original ZIF-8 material. Mao *et al.* developed a ligand-assisted etching process
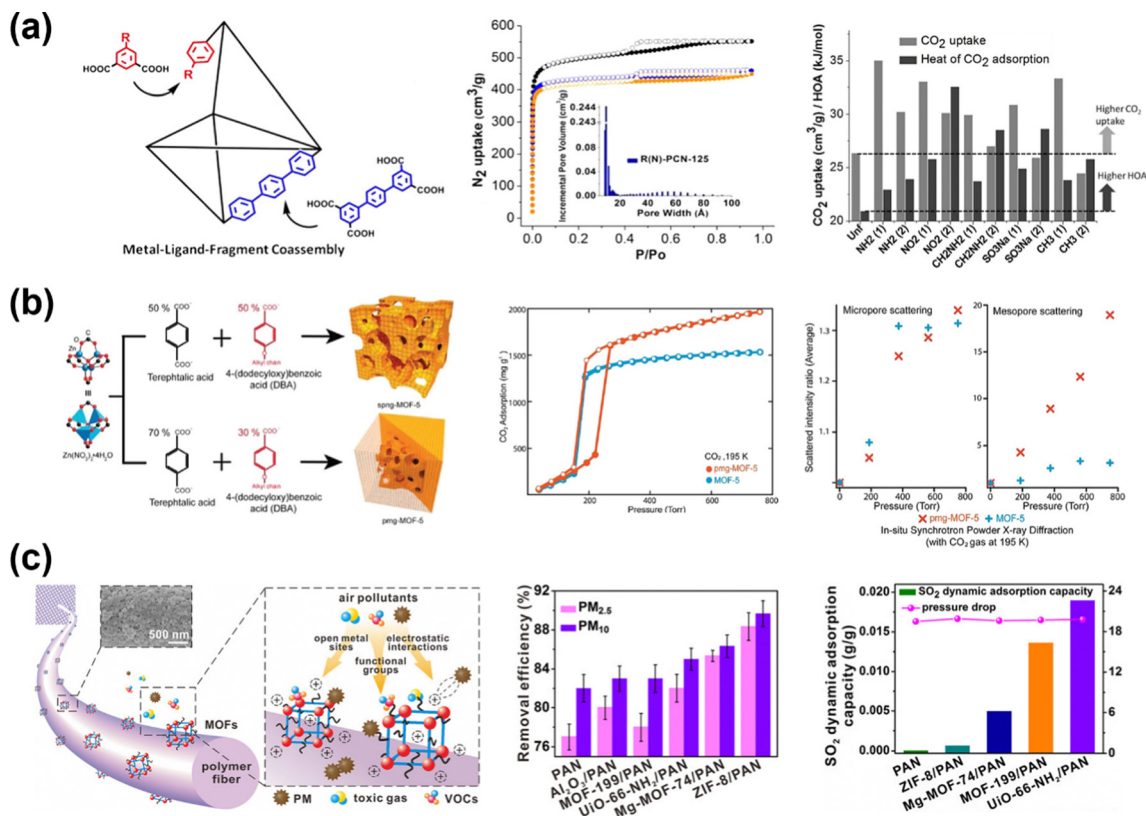
Fig. 8 (a) Mixed-ligand strategy to construct hierarchically porous MOFs that enhance CO_2 adsorption.[125] Reprinted with permission from ref. 125. Copyright 2012, American Chemical Society. (b) Modulator strategy to construct hierarchically porous MOFs that enhance CO_2 adsorption.[21] Reprinted with permission from ref. 21. Copyright 2011, American Chemical Society. (c) MOF composites to enhance SO_2 adsorption.[136] Reprinted with permission from ref. 136. Copyright 2016, American Chemical Society.

for the template-free synthesis of hierarchical single-crystal HKUST-1 at 313 K.[127] It was shown that the CO_2 adsorption of hierarchically porous HKUST-1 is ∼1.5 times higher than the original HKUST-1 material at 223 K and 20 kPa. Even at 323 K and 20 kPa, the CO_2 adsorption was 25% higher than that of pristine HKUST-1. Moreover, the mesoporous structure enhances the CO_2 diffusion and mass transfer rate. In addition, modulator and template strategies have been used to enhance the CO_2 adsorption capacity.[21,128,129] For example, Choi et al. demonstrated the highly crystalline hierarchical structures of spng-MOF-5 (sponge structure) and pmg-MOF-5 (pomegranate structure) and investigated the CO_2 adsorption properties of these hierarchically porous MOFs.[21] Although the surface area of pmg-MOF-5 (3230 $m^2 g^{-1}$) was smaller than that of MOF-5 (3410 $m^2 g^{-1}$), pmg-MOF-5 (CO_2: 2.0 g g^{-1} at 195 K and 760 torr) adsorbs more CO_2 than MOF-5 (CO_2: 1.5 g g^{-1} at 195 K and 760 torr). When comparing the adsorption isotherms of CO_2 at 195 K, pmg-MOF-5 forms an adsorption hysteresis loop between 160 torr and 220 torr that was not observed for MOF-5 and the amount of CO_2 adsorbed was significantly higher, as shown in Fig. 8b. In situ synchrotron powder X-ray diffraction analysis of the gas adsorption process showed that pmg-MOF-5 has scattered X-ray peaks corresponding to CO_2 adsorbed in the micropores and mesopores. In contrast, MOF-5 has scattered X-ray peaks for CO_2 adsorbed in the micropore region only.

The additional CO_2 adsorption in the mesopores and macropores of pmg-MOF-5 was confirmed. Wang et al. obtained hierarchically porous HKUST-1 with micro–meso–macropores upon adding compressed CO_2 during the synthesis process.[130] The obtained hierarchically porous HKUST-1 can be used for the selective adsorption of CO_2 and CH_4. The results showed that the adsorption of CH_4 increased compared to the original HKUST-1 material, but was much lower than the increased adsorption of CO_2. Due to the larger quadrupole moment of CO_2 molecules and lower adsorption energy of CH_4 molecules at the Cu sites, CO_2 has a higher adsorption capacity than CH_4.[131]

In addition, MOFs can also be combined with porous materials to enhance their adsorption capacity for CO_2. Rosi et al. reported a core–shell MOF with a hierarchical structure comprised of a bio-MOF-11/14 hybrid core and bio-MOF-14 shell used for CO_2 adsorption.[132] The core–shell MOF comprised of bio-MOF-11/14@bio-MOF-14 showed 30% higher CO_2 adsorption than bio-MOF-14, but lower N_2 adsorption than the bio-MOF-11/14 core. When the core–shell structure was disrupted by grinding the fractured microcrystals, the N_2 adsorption amount doubled, but the CO_2 adsorption capacity remained the same. It was shown that the bio-MOF-14 shell has a significant inhibitory effect on N_2 adsorption and no effect on CO_2 adsorption, combining the advantages of bio-MOF-11 (high CO_2 adsorption capacity) and bio-MOF-14 (high CO_2/N_2 selectivity

and water stability). Singh *et al.* reported the core–shell synthesis ZIF-8@ZIF-67 and ZIF-67@ZIF-8 with enhanced H_2 storage performance (2.03 and 1.69 wt%) at 77 K and 1 bar, which was approximately 41 and 18% higher than that of ZIF-8, respectively. In addition, the CO_2 uptake of the core–shell ZIF-8@ZIF-67 structure (1.67 mmol g^{-1}, 7.35 wt%) was two times higher than that of the core ZIF-8 material (0.83 mmol g^{-1}, 3.65 wt%) and also higher than that of the shell ZIF-67 material (1.11 mmol g^{-1}, 4.91 wt%).[133] Kim *et al.* prepared a graphene/ZIF-8 nanocomposite with tunable porosity and surface area, where the distribution of micro–mesopores and the crystal size of ZIF-8 can be controlled by simply varying the annealing temperature of graphene oxide (GO).[134] The specific surface area of GO/ZIF-8 was 720.0 m^2 g^{-1} and the CO_2 adsorption at 35 bar and 303 K was 17 mmol g^{-1}, which is much higher than the CO_2 adsorption measured under the same conditions for ZIF-8 with a specific surface area of 1871 m^2 g^{-1} (8.5 mmol g^{-1}), indicating that the synergistic effect between graphene and ZIF-8 can enhance the CO_2 adsorption capacity, while the gas molecules can be rapidly mass transferred to the adsorbent *via* the mesopores. Pressure swing adsorption (PSA) usually requires relatively high pressure to capture and store CO_2, so the GO/ZIF-8 nanocomposite is more favorable for application in PSA than ZIF-8.

Hierarchically porous MOFs with macroporous structures are generally not used for gas adsorption, but are typically used for the adsorption of organic molecules and catalysis. Hierarchically porous MOFs are widely used to enhance the gas adsorption capacity. For example, Wisser *et al.* used chitinous material obtained from sponges as a carrier for MOFs and this composite has a hierarchically porous structure.[135] The specific surface area of the composite prepared with a 53% (w/w) loading of HKUST-1 was up to 800 m^2 g^{-1}, where the structure of the mesopores depends on the structure of the chitinous pores. Ammonia penetration experiments showed the good adsorption kinetics of the composites. Moreover, SO_2 is one of the major gaseous pollutants harmful to the ecosystem. Zhang *et al.* adsorbed SO_2 by compositing MOFs with polyacrylonitrile (PAN) into hierarchically porous materials.[136] Because MOFs have more binding sites than PAN, the MOF-199/PAN and UiO-66-NH_2/PAN composites adsorb SO_2 more effectively when compared to pure PAN, as shown in Fig. 8c. The N_2 isotherms are typical type II curves. Penetration tests indicate that the hierarchically porous structures in the composites enhance the mass transfer rate. In addition to the gases mentioned above, PM (particulate matter) is one of the main gaseous pollutants found in the environment.[137] Wang and co-workers reported a roll-to-roll hot-pressing method for the large-scale production of different MOF composites used for PM adsorption.[138] The PM removal efficiency of ZIF-8@Plastic with a hierarchically porous structure was improved by a factor of four when compared to the original plastic mesh.

3.2 Adsorption of other molecules

In terms of environmental pollution, heavy metals such as mercury, cadmium, lead, chromium, and arsenic, are biotoxic and significant pollutents. Low concentrations of heavy metal ions can accumulate in living organisms causing heavy metal poisoning and carcinogenesis, which can have fatal effects on humans.[139,140] Since hierarchically porous MOFs are usually considered promising materials for the adsorption of hazardous substances due to their simultaneous multiple pore properties,[15] the application of hierarchically porous MOFs has been investigated for adsorption of arsenic[141,142] and heavy metal ions, such as chromium,[26] lead,[143] and cadmium. Liu *et al.* proposed a strategy to prepare UiO-66-NH_2-CS aerogels (UNCAM) with hierarchical structures.[25] UNCAM exhibited higher mass transfer rates than UiO-66-NH_2 powder, as shown in Fig. 9a. The adsorption capacity for Pb(II) increased with an increase in the UiO-66-NH_2 content in UNCAM. The adsorption capacity of UNCAM was still >90% after three cycles. Wu *et al.* investigated the synthesis of ZIF-8 with a double microporous–mesoporous structure using cetyltrimethylammonium bromide (CTAB) and L-histidine (His) as co-templates in water at room temperature.[144] Experiments on the static adsorption of arsenate revealed that the As^V ion adsorption capacity of the hierarchical structured ZIF-8 (H-ZIF-8-14) prepared with a CTAB : His molar ratio of 1 : 4 was ~1.8 times higher than that of ZIF-8 synthesized in an aqueous system. This may be attributed to ZIF-8 with mesoporous structures has higher porosity, which facilitates mass transfer and increases the contact area with arsenate. The arsenate adsorption capacity of hierarchically porous ZIF-8 was maintained after three adsorption–desorption cycles. Some MOF-on-MOF structures can enhance the mass transfer and adsorption of macromolecules. For example, Mutruc *et al.* developed a two-component core–shell MOF based on UiO-68, which consists of a core that stores the guest molecule and an azobenzene-ligand shell that photoisomerizes to control the uptake and release of

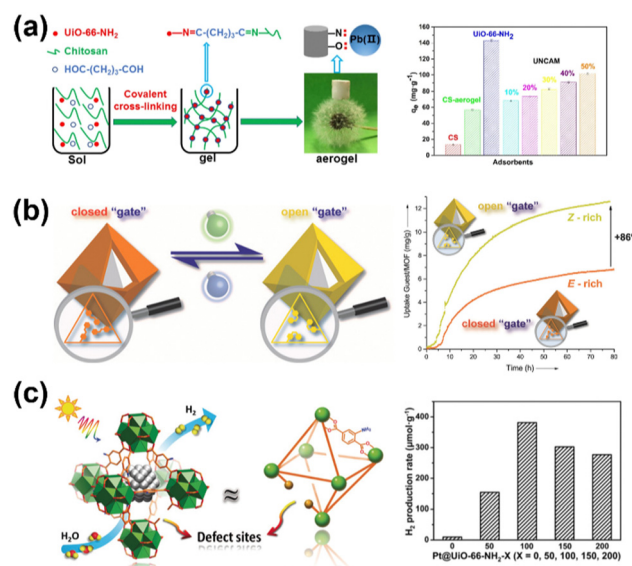Fig. 9 (a) Hierarchically porous UiO-66-NH_2 aerogel adsorbs Pb(II).[25] Reprinted with permission from ref. 25. Copyright 2020, Elsevier. (b) Core–shell structured MOF adsorbs macromolecules.[145] Reprinted with permission from ref. 145. Copyright 2019, Wiley. (c) Hierarchically porous UiO-66-NH_2 improves catalytic efficiency.[27] Reprinted with permission from ref. 27. Copyright 2019, Wiley.

Table 1 Summary of hierarchically porous MOFs constructed by different strategies

Scale	Strategy	MOFs	Metal with linker, additives	Pore diameter (nm)	Control methods	Application	Ref.
Micro–micro porous	Mix metals	UiO-66	Zr, Ti with BDC	0.5–1	The molar ratio of metals mixture	CO_2 absorption	48
		MOF-74	Mg, Ca, Sr, Ba, Mn, Fe, Co, Ni, Zn, Cd with DOT	—	The molar ratio of metals mixture	—	49
	Mix linkers	MOF-5	Zn with BDC, BDC-NH_2, BDC-Br, BDC-$(Cl)_2$, BDC-NO_2, BDC-$(CH_3)_2$, BDC-C_4H_4, BDC-$(OC_3H_5)_2$, BDC-$(OC_7H_7)_2$	0.5–1.1	The molar ratio of linkers mixture	CO_2, CO absorption	50
		MOF-5	Zn with BDC, BDC-NH_2	—	The molar ratio of linkers mixture	Benzene, toluene, *para*-xylene, *meta*-xylene, *ortho*-xylene diffusion	46
		UiO-66	Zr with BDC, L-serine	—	The molar ratio of linkers mixture	CO_2 absorption	53
		ZIF-8	Zn with MeIM, IIM, BrIM, ClBIM	—	Type of functional groups	CO_2/N_2, CH_4/N_2 adsorption	126
Micro–mesoporous	Mix linkers	PCN-125	Cu with TPTC, H-isoph, CH_3-isoph, NH_2-isoph, CH_2NH_2-isoph, NO_2-isoph, SO_3H-isoph, SO_3Na-isoph	2–30	The molar ratio of linkers mixture	CO_2 absorption	125
		$Ru_3(btc)_2Cl_{1.5}$	Ru with BTC, pyridine-3,5-dicarboxylate	—	The molar ratio of linkers mixture	CO_2, CO and H_2 absorption; catalytic hydrogenation of 1-octene	52
		MIL-125	Ti with BDC, BDC-NH_2	2–50	The molar ratio of linkers mixture	Toluene adsorption; photodegradation process of toluene	51
	Post-treatment	PCN-160	Zr with AZDC, CBAB	2.5–19	Exchange ratio and acetic acid concentration	accessibility of enzymes; oxidation of ABTS and *o*-phenylenediamine (*o*-PDA)	58
		UiO-66, UiO-67, MOF-5, MIL-125(Ti), MIL-53(Fe)	Zr with BDC; Zr with BPDC; Zn with BDC; Ti with BDC; Fe with BDC	5.5–13	Thermolabile linker ratio, temperature and heat time	Meerwein–Ponndorf–Verley (MPV) reaction	59
		UiO-66, ZIF-8, UiO-67, UiO-66(Hf)	Zr with BDC, TCPP, CoPc; Zr with BPDC; Zn with MeIM; Hf with BDC	2–4.5	The time of laser exposure and ratio of photolabile/robust linkers	—	152
		POST-66(Y), POST-66(Dy), POST-66(Tb), MOF-177(Zn), UiO-67(Zr), MIL-100(Al),	Y with H_3hmtt; Dy with H_3hmtt; Tb with H_3hmtt; Zn with BTB; Zr with BPDC; Al with BTC	3.8 and 6.2–16	Etching temperature, time	VB_{12}, Cyt *c*, myoglobin, HRP absorption; catalytic activity of co-oxidation of 4-aminoantiprine (4-AAP) and phenol	61
		HKUST-1	Cu with BTC	3–30	Treatment time	Thiophene adsorption	62
		HKUST-1	Cu with BTC, hydroquinone	3.8 and (2–50)	—	CO adsorption	63
		HKUST-1	Cu with BTC, NH_3 gas	9.2–38	Etching temperature and amount of the etchant	Encapsulation of methylene blue	23
		HKUST-1, ZIF-67	Cu with BTC; Co with MeIM	3.2 and (2–50)	—	Cycloaddition of CO_2 with epoxides to produce cyclic carbonates	149
		PCN-250	Fe, Ni, Mn, Co, Al, In, Sc with ABTC	4 and (2–50)	Type of metal clusters and decarboxylation temperature	CH_4, CO_2 adsorption	150
		UiO-66, UiO-67, MOF-808, MIL-53	Zr with BDC, sodium acetate, sodium formate, sodium propionate, sodium benzoate; Zr with BPDC; Zr with BTC; Al with BDC	2–30	Type and amount of solution	CO_2 absorption; methyl orange absorption; catalytic cycloaddition reactions between CO_2 and epoxides with different sizes, one-pot cascade synthesis of secondary arylamines	57
	Modulator	UiO-66, UiO-66-NH_2, UiO-66-NO_2, UiO-67, MIL-53, MIL-53-NH_2, DUT-5, MOF-808	Zr with BDC, acetic acid, octanoic acid, dodecanoic acid, palmitic acid; Zr with NH_2-BDC; Zr with NO_2-BDC; Zr with BPDC; Al with BDC; Al	2–8	Molar ratio of reactant and length of modulator	Coomassie brilliant blue R250 absorption; ring opening of styrene oxide with methanol, cycloaddition reactions	67

Table 1 (*continued*)

Scale	Strategy	MOFs	Metal with linker, additives	Pore diameter (nm)	Control methods	Application	Ref.
			with NH_2-BDC; Al with BPDC; Zr with BTC			between 1,3-cyclohexanedione and α,β-unsaturated aldehydes	
		UiO-66	Zr with BDC, acetic acid	1.7 and 16	Process of crystallization and concentration of modulator	Isomerization of glucose to fructose	64
		UiO-66	Zr with BDC, trifluoroacetic acid	1.6 and >20	Aging time	Cyclohexanone conversion to cyclohexanol	69
		UiO-66-NH_2	Zr with NH_2-BDC, acetic acid	1.5–50	Amount of the modulator	Photocatalytic H_2 from water splitting	27
		HKUST-1	Cu with BTC, acetic acid	2–15 and >25	Amount of the modulator	CH_4 absorption	65
		HKUST-1	Cu with BTC, benzoic acid	∼14.8	—	—	68
		PCN-250	Fe with ABTC, propanoic acid, hexanoic acid, nonanoic acid, myristic acid	4–18	The length and concentration of the fatty acid	Methylene blue absorption	66
	Template	HKUST-1	Cu with BTC, CTAB	3.8–31	Molar ratio of template	—	70
		HKUST-1	Cu with BTC, CTAB, citric acid	3–30	Molar ratio of template	—	72
		HKUST-1	Cu with BTC, CTAB, 1,3,5-trimethyl benzene	4–25	Type of template and molar ratio of template	CO_2 adsorption; oxidation of benzyl alcohol to benzaldehyde	74
		MIL-100, MIL-96, MIL-110	Al with BTC, CTAB	3–33	pH value and ratio of solvent	—	71
		MFM-100, HKUST-1, MOF-2	Cu with biphenyl-3,3′,5,5′-tetracarboxylic acid, $OmimBF_4$; Cu with BTC; Zn with BDC	∼4.7	Molar ratio of template and electrosynthesis	Catalytic activity of alcohol oxidation	76
		HKUST-1, Mn-BTC, Mn-BDC	Cu with BTC, CO_2-expanded liquid; Mn with BTC; Mn with BDC	13–23	Molar ratio of template (CO_2 pressure) and type of solvent	Oxidation of benzyl alcohol to benzaldehyde	77
		UiO-66, HKUST-1	Zr with BDC, poly(ethylene glycol)-based alkylammonium and bromide ionic liquid; Cu with BTC	2–50	Temperature and time of synthesis	Encapsulation of Cyt *c*	151
	Nucleation kinetics	UiO-66(Hf), UiO-66, UiO-66-OH_2(Hf), UiO-66-NH_2(Hf), NUS-6(Hf)	Hf with BDC; Zr with BDC; Hf with OH_2-BDC; Hf with NH_2-BDC; Hf with SO_3Na-BDC	3.7–16.6	Molar ratio of solvent	Tetrakis (4-carboxyphenyl)-porphyrin absorption; catalytic methanolysis of styrene oxide	80
		Zn-MOF-74	Zn with DOT	5–20	Time of synthesis	Brilliant Blue R-250 absorption	78
	MOF composites	PCN-222@PS, PCN-160(Zr)@PS, PCN-224(Zr)@PS, MOF-801(Zr)@PS, PCN-900(Eu)@PS	Zr with TCPP, Zn with BDC, tetrasodium ethylenediaminetetraacetate, PS; Zr with AZDC; Zr with TCPP; Zr with fumaric acid; Eu with TCPP	—	—	—	84
		PCN-222/PCN-608, /NU-1000, /PCN-134, Zr-BTB/PCN-134	Zr with TCPP, TCPB-OH; Zr with TBAPy; Zr with TCPP, BTB	<5	—	—	82
		PCN-222@UiO-67, PCN-134@Zr-BTB, PCN-222@Nu-1000, PCN-222@Zr-AZDC, PCN-222@Zr-NDC, La-TCPP@La-BPDC	Zn with TCPP, Zr with BPDC; Zr with BTB; Zr with TBAPy; Zr with AZDC; Zr with NDC; La with TCPP, La with BPDC	<5	—	Catalyze epoxidation of alkenes	88
		Co, Fe-MOF-74/Co/carbon cloth	Co, Fe with DOT, carbon cloth	—	Molar ratio of metal salt	Electrocatalytic splitting water	85
		PMMA@IRMOF-3@MOF-5	Zn with BDC, BDC-NH_2, PMMA	—	Time of polymerization	—	86
		UiO-66@ZIF-8, Pd-UiO-66-NH_2@ZIF-8	Zr with BDC, Zn with MeIM, CTAB, PVP, SiO_2; Pd, Zr with BDC-NH_2, Zn with MeIM	—	—	Ethylene hydrogenation	83
		NH_2-UiO-66@NH_2-MIL-125, MOF-76@NH_2-MIL-125, MIL-	Zr, Ti with BDC-NH_2, PVP; Tb with BTC; Cr with BDC	—	—	Cr^{VI} adsorption; photocatalytic Cr^{VI} reduction	26

Table 1 (continued)

Scale	Strategy	MOFs	Metal with linker, additives	Pore diameter (nm)	Control methods	Application	Ref.
		101@NH$_2$-MIL-125, NH$_2$-UiO-66 & MOF-76@NH$_2$-MIL-125					
		ZIF-67@ZIF-8	Zn, Co with MeIM	—	—	H$_2$ storage, CO$_2$ adsorption	133
		M$_2$(ndc)$_2$(dabco) (M = Co, Ni, Cu, Zn)	Co, Ni, Cu, Zn with NDC, dabco	5–>20	—	Methane, ethane, ethene, propane, propene adsorption	119
		ZIF-67@Yeast	Co with MeIM, yeast	—	—	Pb^{2+} adsorption	143
		Polyacrylonitrile/UiO-66	Zr with BDC, polyacrylonitrile	2.5–10	—	H$_2$ storage	122
		Chitin fibers/HKUST-1	Cu with BTC, chitin fibers	—	—	NH$_3$ adsorption	135
		ZIF-8/PAN, Mg-MOF-74/PAN, UiO-66-NH$_2$/PAN, MOF-199/PAN	Zn with MeIM, PAN; Mg with DOT; Zr with H$_2$N-BDC; Cu with BTC	—	—	Particulate matter, SO$_2$ adsorption	136
	Gelation	Cr, Fe-BTC, BDC, NDC, ADC, FDC, BuDC, BTB	Cr, Fe with BTC, BDC, NDC, ADC, FDC, BuDC, BTB, BPDC	3–33	Molar ratio of reactant, temperature	Methyl orange, dimethyl phthalate, methylene blue adsorption	90
Micro–macroporous	Template	ZIF-8	Zn with MeIM, PS	190–470	Particle size of template	Knoevenagel reaction between benzaldehydes and malononitriles	28
	3D printing	MOF-5	Cu with BTC, acrylonitrile butadiene styrene	(>50)	—	H$_2$ storage	112
Micro–meso–macroporous	Post-treatment	UiO-66	Zr with BDC, acetate, formate, propionate, benzoate	3–70	The length of the monocarboxylic acid, etching temperature and amount of the etchant	Cytochrome c, horse radish peroxidase absorption	60
		HKUST-1, MOF-5	Cu with BTC; Zn with BDC	30–260	Etching temperature, time, molar ratio of solvent	CO$_2$ adsorption	127
	Modulator	MOF-5	Zn with BDC, 4-(dodecyloxy)benzoic acid	10–100	Molar ratio of reactant	CO$_2$ absorption	21
	Template	HKUST-1, Al-MIL-96	Cu with BTC, CO$_2$-expanded liquid; Al with BTC, F127	∼25 and 68–106	Molar ratio of template (CO$_2$ pressure), molar ratio of solvent	CH$_4$, CO$_2$ adsorption; methylene blue adsorption	130
		HKUST-1, CuBDC	Cu with BTC, PS, citrate/CTAB; Cu with BDC	∼20 and 80–400	Particle size of template	Methylene blue adsorption; accelerate Friedländer reaction between 2-aminobenzophenones and acetylacetone, hydrolyse the ester in water	147
		MIL-101	Cr with BDC, CTAB	5–100	Molar ratio of template	Methene blue adsorption	123
		ZIF-8, ZIF-90	Zn with MeIM, N,N-diethylethanolamine; Zn with imidazole-2-carboxaldehyde	5–100	Molar ratio of template	CO$_2$ adsorption	128
		UiO-66(Ce)	Ce with BDC, P123/F127	20–110 and >1000	Molar ratio of template	DNA adsorption; catalyze the hydrolysis of the high-energy phosphate bonds	24
		Cu-BDC	Cu with BDC, PS, P123	3.9 and 455	Particle size of template	CO$_2$ adsorption; CO$_2$ carbonylative coupling reaction with 4-methylbenzyl chloride	129
	Nucleation kinetics	ZIF-8	Zn with MeIM	10–60	Molar ratio of reactant	CO$_2$ adsorption; methylene blue, methyl blue, rhodamine B absorption	124
		HKUST-1	Cu with BTC	26–72	Temperature of synthesis	Electrocatalytic oxygen reduction reaction	79
	MOF composites	Graphene/ZIF-8	Zn with MeIM, graphene	3.7 and 10–100	Temperature of thermally annealed	CO$_2$ adsorption	134
	Gelation	MIL-100(Fe)	Fe with BTC	3–4.5 and >50	Molar ratio of linkers	CH$_4$ adsorption	89
		MIL-53(Al), Al-BTC	Al with BDC, CTAB, TMB; Al with BTC	5.4–87.8	Gelation temperature, reactant concentration	H$_2$ storage, CO$_2$ adsorption; benzene, n-hexane, methanol adsorption; congo red, brilliant blue R-250 adsorption	22
		UiO-66-NH$_2$	Zr with BDC-NH$_2$	—	—	Pb^{2+}	25
		MOF-5	Zn with BDC	<200			92

Table 1 (*continued*)

Scale	Strategy	MOFs	Metal with linker, additives	Pore diameter (nm)	Control methods	Application	Ref.
	Mechanosynthesis				Molar ratio of reactant, grinding speed and time	Methane, ethane, propane, *n*-butane, *n*-pentane, *n*-hexane, *n*-heptane absorption	
		HKUST-1	Cu with BTC	—	Molar ratio of solvent, treatment time	Benzene absorption	93
		HKUST-1	Cu with BTC, NaCl, KCl, triethylenediamine	2–100	Molar ratio of reactant	I_2 adsorption	99
		ZIF-8	Zn with MeIM	10–100	Molar ratio of reactant	*n*-Butanol and hexane adsorption; rhodamine B adsorption	100
		ZIF-1, ZIF-3, ZIF-4, ZIF-8	Zn with imidazole; Zn with MeIM	10–100	—	—	96
		Zn-MOF-74	Zn with DOT	—	Type of solvent	—	101
	3D printing	HKUST-1	Cu with BTC	(2–50 and > 50)	—	CH_4 adsorption	120
		HKUST-1	Cu with BTC, PVA, bentonite clay, methyl-cellulose	2.9–9.1 and (50)	Synthesis temperature and activation solvent	CO_2 adsorption	108
		MOF-74(Ni), UTSA-16(Co)	Ni with DOT, bentonite clay, poly(vinyl alcohol); Co with citric acid	10–50 and (> 50)	—	CO_2 adsorption	106
		ZIF-8 (MIL-100(Fe))	Zn with MeIM, TOCNF, curcumin, alginate	2–50 and (> 50)	MOF contents	Curcumin release	110

BDC = 1,4-benzenedicarboxylate; BTC = 1,3,5-benzenetricarboxylate; DOT = 2,5-dioxidoterephthalate; BPDC = 4,4′-biphenyl-dicarboxylate; TPTC = terphenyltetracarboxylate; isoph = isophthalic acid; MeIM = 2-methylimidazole; IIM = 4-iodoimidazole; BrIM = 4-bromoimidazole; ClBIM = 2-chloromethylbenzimidazole; AZDC = azobenzene-4,4′-dicarboxylate; CBAB = 4-carboxybenzylidene-4-aminobenzate; TCPP = tetrakis(4-carboxyphenyl)porphyrin; CoPc = cobalt tetra(carboxy)phthalocyanine; H_3hmtt = methyl substituted truxene tricarboxylic acid; VB_{12} = Vitamin B_{12}, Cyt *c* = cytochrome *c*, HRP = horseradish peroxidase; BTB = 1,3,5-benzenetribenzoic acid; ABTC = 3,3′,5,5′-azobenzenetetracarboxylic; $OmimBF_4$ = 1-octyl-3-methylimidazolium tetrafluoroborate; PS = polystyrene; TPCB-OH = 3,3′,5,5′-tetrakis(4-carboxyphenyl)-4,4′-dihydroxybiphenyl; TBAPy = 1,3,6,8-tetrakis(4-benzoicacid)pyrene; NDC = naphthalene dicarboxylate; PMMA = poly(methyl methacrylate); dabco = 1,4-diazabicyclo[2.2.2]octane; H2BuDC = 5-*tert*-butylisophthalic acid; FDC = fumaric acid; ADC = 5-aminoisophthalic acid; TMB = 1,3,5-trimethylbenzene; TOCNF = anionic 2,2,6,6-tetramethylpiperidine-1-oxylradical-mediated oxidized cellulose nanofibers.

the guest molecule.[145] The results obtained from 1-pyrene carboxylic acid adsorption experiments showed that the adsorption and release properties can be effectively modulated by tuning the photo-responsive azobenzene shell, as shown in Fig. 9b. In addition to the adsorption of organic macromolecules and immobilization of biological macromolecules such as enzymes, DNA, and proteins can be achieved by expanding the pore size of the mesopores in hierarchically porous MOFs.[36] Enzymes encapsulated in MOFs have higher catalytic activity.[146] These examples demonstrate that introducing larger pores into pristine microporous MOFs can be used to encapsulate macromolecules.

3.3 Catalysis

MOFs are widely used in multiphase catalysis, but usually the pore sizes of MOFs are regulated in the micropore range, thus, slowing the diffusion rate and limiting the catalytic reactions of large molecules.[40] Hierarchically porous MOFs are usually constructed using defects to enhance the mass transfer and have exposed active sites, which can improve the catalytic efficiency of UiO-66-NH$_2$, as shown in Fig. 9c.[27] Cui *et al.* proposed a method to prepare highly monodisperse HKUST-1 with cubic shape and a hierarchically porous structure based on a microfluidic strategy.[147] Their experiments found that when compared with microporous HKUST-1, monocrystalline

HKUST-1 with a hierarchically porous structure can accelerate the Friedländer reaction between 2-amino benzophenone and acetylacetone, indicating that hierarchically porous HKUST-1 accelerated the mass transfer and enhanced the catalytic efficiency. Zhang *et al.* reported the synthesis of Pt/ZIF-8 with a hierarchically porous structure using Au nanoparticles as hard templates (followed by etching with solutions of KI and I_2).[148] This strategy of constructing hierarchically porous ZIF-8 can regulate the nature of mesopores by adjusting the size, shape, and spatial distribution of the Au nanoparticles, while not destroying the original crystal structure. It was found that Pt/ZIF-8 with a hierarchically porous structure showed significantly higher conversions in the catalytic liquid-phase hydrogenation of *n*-pentene, *n*-hexene, *n*-heptene, and *cis*-cyclooctene, indicating that the mesopores in Pt/ZIF-8 with a hierarchically porous structure improved the diffusion rate of the molecules and maintained its molecular sieving selectivity.

4 Conclusion and outlook

Because microporous MOF materials are used in adsorption and separation, there are problems related to their slow mass transfer rates and active sites being confined to the micropores. The introduction of larger pores in the presence of micropores can improve the mass transfer efficiency and even the

utilization of active sites. Therefore, each strategy used for the construction of hierarchically porous MOFs based on the pore size introduced have been summarized and some examples of their applications in adsorption-diffusion are presented (Table 1).

Methods that introduce pores whose pore sizes are usually micropores mainly replacing part of the metal or ligand in the MOF. Usually, the effect of replacing the metal on the MOF pore size is minimal. Still, this approach changes the active sites and has an impact on the adsorption performance. Under the condition of ensuring the same topology, the choice of the replacement ligand mostly involves the use of a derivatized ligand bearing different functional groups, so the change in the pore size is usually smaller than the original pore. However, mixed ligands sometimes have the phenomenon of missing ligands, which cannot only improve diffusion, but also introduce different functional groups to change the active sites. There is still a lack of sufficient knowledge to apply this approach to construct mesopores. There are three mechanisms in the methods used to introduce mesopores, including the introduction of defects, nucleation kinetics, and combination of other porous materials (including MOFs). Constructing mesoporous MOFs by introducing defects usually requires the MOFs to be structurally stable before and after the introduction of the defects in order to obtain homogeneous pore sizes. The strategies used to form mesopores *via* introducing defects include post-treatment, modulator, and template strategies. Among them, post-treatment can easily construct hierarchically porous structures in different MOFs. The modulator strategy is often applied to partial MOFs bearing carboxylic acid ligands. Although the template strategy usually forms relatively uniform mesopores, the problem of repelling the templates during the crystal growth process of MOFs and the additional steps required to remove the template need to be addressed (the removal of the template may lead to the collapse of the uniform mesopores formed during this process). The nucleation kinetics strategy enables the formation of tunable mesopores by changing the synthesis conditions, but at the expense of the MOF crystallinity. In addition, MOFs composites can combine the characteristics of two porous materials in addition to introducing different pore sizes, *e.g.*, MOF composites with carbon materials can significantly enhance the CO_2 adsorption performance. Methods that usually introduce macropores mainly include mechanosynthesis and gelation. The mechanosynthesis strategy is a green and economic approach that can synthesize MOFs in large quantities. MOFs gelation and 3D printed MOFs are both molding processes. In addition, the 3D printing strategy can fabricate MOFs monolithic materials and precisely control the pore size of the macropores. It is expected that after 3D printing technology is upgraded, work on 3D printed and accurately customized MOFs structures will be seen.

Despite the extensive work fabricating hierarchically porous MOFs, three main challenges still need to be addressed. One is to meet the requirements of their industrial production and find a general method for the green synthesis and reproducible construction of hierarchically porous MOFs. The second is to synthesize hierarchically porous MOFs with uniform and highly ordered porous structures. The third is the effect of activation on the structural stability of the hierarchically porous MOFs. In addition, there are few reports on the construction of hierarchically porous MOFs with multiple strategies and it is speculated that micro–meso–macroporous MOF materials can be constructed through the combination of multiple strategies. In conclusion, the extensive application of hierarchically porous MOFs in adsorption-diffusion validates that the strategy of constructing hierarchically porous MOFs to improve the mass transfer rate of microporous MOFs is feasible.

Conflicts of interest

There are no conflicts to declare.

Acknowledgements

References

1 O. K. Farha, C. E. Wilmer, I. Eryazici, B. G. Hauser, P. A. Parilla, K. O'Neill, A. A. Sarjeant, S. T. Nguyen, R. Q. Snurr and J. T. Hupp, Designing higher surface area metal-organic frameworks: are triple bonds better than phenyls?, *J. Am. Chem. Soc.*, 2012, **134**, 9860–9863.

2 C. Liu, T. Y. Luo, E. S. Feura, C. Zhang and N. L. Rosi, Orthogonal Ternary Functionalization of a Mesoporous Metal-Organic Framework via Sequential Postsynthetic Ligand Exchange, *J. Am. Chem. Soc.*, 2015, **137**, 10508–10511.

3 X. C. Huang, Y. Y. Lin, J. P. Zhang and X. M. Chen, Ligand-directed strategy for zeolite-type metal-organic frameworks: zinc(II) imidazolates with unusual zeolitic topologies, *Angew. Chem., Int. Ed.*, 2006, **45**, 1557–1559.

4 Y. Chen, T. Hoang and S. Ma, Biomimetic catalysis of a porous iron-based metal-metalloporphyrin framework, *Inorg. Chem.*, 2012, **51**, 12600–12602.

5 A. Schaate, P. Roy, A. Godt, J. Lippke, F. Waltz, M. Wiebcke and P. Behrens, Modulated Synthesis of Zr-Based Metal–Organic Frameworks: From Nano to Single Crystals, *Chem. – Eur. J.*, 2011, **17**, 6643–6651.

6 H. C. Zhou, J. R. Long and O. M. Yaghi, Introduction to metal-organic frameworks, *Chem. Rev.*, 2012, **112**, 673–674.

7 J. R. Long and O. M. Yaghi, The pervasive chemistry of metal-organic frameworks, *Chem. Soc. Rev.*, 2009, **38**, 1213–1214.

8 T. Ben, C. Lu, C. Pei, S. Xu and S. Qiu, Polymer-Supported and Free-Standing Metal–Organic Framework Membrane, *Chem. – Eur. J.*, 2012, **18**, 10250–10253.

9 T. J. Reade, T. S. Murphy, J. A. Calladine, R. Horvath, I. P. Clark, G. M. Greetham, M. Towrie, W. Lewis,

M. W. George and N. R. Champness, Photochemistry of framework-supported M(diimine)(CO)₃X complexes in three-dimensional lithium carboxylate metal-organic frameworks: monitoring the effect of framework cations, *Philos. Trans. R. Soc., A*, 2017, **375**, 20160033.

10 J. Zhou, P. Wang, C. Wang, Y. T. Goh, Z. Fang, P. B. Messersmith and H. Duan, Versatile Core–Shell Nanoparticle@Metal–Organic Framework Nanohybrids: Exploiting Mussel-Inspired Polydopamine for Tailored Structural Integration, *ACS Nano*, 2015, **9**, 6951–6960.

11 A. H. Assen, O. Yassine, O. Shekhah, M. Eddaoudi and K. N. Salama, MOFs for the Sensitive Detection of Ammonia: Deployment of fcu-MOF Thin Films as Effective Chemical Capacitive Sensors, *ACS Sens.*, 2017, **2**, 1294–1301.

12 F.-X. Coudert and A. H. Fuchs, Computational characterization and prediction of metal–organic framework properties, *Coord. Chem. Rev.*, 2016, **307**, 211–236.

13 H. Park, Y. Kang, W. Choe and J. Kim, Mining Insights on Metal-Organic Framework Synthesis from Scientific Literature Texts, *J. Chem. Inf. Model.*, 2022, **62**, 1190–1198.

14 K. Li, J. Valla and J. Garcia-Martinez, Realizing the Commercial Potential of Hierarchical Zeolites: New Opportunities in Catalytic Cracking, *ChemCatChem*, 2014, **6**, 46–66.

15 D. M. Kabtamu, Y. N. Wu and F. Li, Hierarchically porous metal-organic frameworks: synthesis strategies, structure(s), and emerging applications in decontamination, *J. Hazard. Mater.*, 2020, **397**, 122765.

16 F. G. Cirujano, N. Martin and L. H. Wee, Design of Hierarchical Architectures in Metal–Oganic Frameworks for Catalysis and Adsorption, *Chem. Mater.*, 2020, **32**, 10268–10295.

17 A. Pal, S. Chand and M. C. Das, A Water-Stable Twofold Interpenetrating Microporous MOF for Selective CO₂ Adsorption and Separation, *Inorg. Chem.*, 2017, **56**, 13991–13997.

18 H. Deng, S. Grunder, K. E. Cordova, C. Valente, H. Furukawa, M. Hmadeh, F. Gandara, A. C. Whalley, Z. Liu, S. Asahina, H. Kazumori, M. O'Keeffe, O. Terasaki, J. F. Stoddart and O. M. Yaghi, Large-pore apertures in a series of metal-organic frameworks, *Science*, 2012, **336**, 1018–1023.

19 F. Villemot, A. Galarneau and B. Coasne, Adsorption and Dynamics in Hierarchical Metal–Organic Frameworks, *J. Phys. Chem. C*, 2014, **118**, 7423–7433.

20 F. Chang, J. Zhou, P. Chen, Y. Chen, H. Jia, S. M. I. Saad, Y. Gao, X. Cao and T. Zheng, Microporous and mesoporous materials for gas storage and separation: a review, *Asia-Pac. J. Chem. Eng.*, 2013, **8**, 618–626.

21 K. M. Choi, H. J. Jeon, J. K. Kang and O. M. Yaghi, Heterogeneity within order in crystals of a porous metal-organic framework, *J. Am. Chem. Soc.*, 2011, **133**, 11920–11923.

22 L. Li, S. Xiang, S. Cao, J. Zhang, G. Ouyang, L. Chen and C. Y. Su, A synthetic route to ultralight hierarchically micro/mesoporous Al(ɪɪɪ)-carboxylate metal-organic aerogels, *Nat. Commun.*, 2013, **4**, 1774.

23 M. K. Albolkany, C. Liu, Y. Wang, C. H. Chen, C. Zhu, X. Chen and B. Liu, Molecular Surgery at Microporous MOF for Mesopore Generation and Renovation, *Angew. Chem., Int. Ed.*, 2021, **60**, 14601–14608.

24 J. Yang, K. Li and J. Gu, Hierarchically Macro-Microporous Ce-Based MOFs for the Cleavage of DNA, *ACS Materials Lett.*, 2022, **4**, 385–391.

25 Q. Liu, S. Li, H. Yu, F. Zeng, X. Li and Z. Su, Covalently crosslinked zirconium-based metal-organic framework aerogel monolith with ultralow-density and highly efficient Pb(II) removal, *J. Colloid Interface Sci.*, 2020, **561**, 211–219.

26 Y. Gu, Y.-n Wu, L. Li, W. Chen, F. Li and S. Kitagawa, Controllable Modular Growth of Hierarchical MOF-on-MOF Architectures, *Angew. Chem., Int. Ed.*, 2017, **56**, 15658–15662.

27 X. Ma, L. Wang, Q. Zhang and H. L. Jiang, Switching on the Photocatalysis of Metal-Organic Frameworks by Engineering Structural Defects, *Angew. Chem., Int. Ed.*, 2019, **58**, 12175–12179.

28 K. Shen, L. Zhang, X. Chen, L. Liu, D. Zhang, Y. Han, J. Chen, J. Long, R. Luque, Y. Li and B. Chen, Ordered macro-microporous metal-organic framework single crystals, *Science*, 2018, **359**, 206–210.

29 J. Yang, J. Liu, P. Liu, L. Li, X. Tang, H. Shang, J. Li and B. Chen, K-Chabazite Zeolite Nanocrystal Aggregates for Highly Efficient Methane Separation, *Angew. Chem., Int. Ed.*, 2022, **61**, e202116850.

30 X. Y. Yang, L. H. Chen, Y. Li, J. C. Rooke, C. Sanchez and B. L. Su, Hierarchically porous materials: synthesis strategies and structure design, *Chem. Soc. Rev.*, 2017, **46**, 481–558.

31 H.-Y. Guan, R. J. LeBlanc, S.-Y. Xie and Y. Yue, Recent progress in the syntheses of mesoporous metal–organic framework materials, *Coord. Chem. Rev.*, 2018, **369**, 76–90.

32 D. Liu, D. Zou, H. Zhu and J. Zhang, Mesoporous Metal-Organic Frameworks: Synthetic Strategies and Emerging Applications, *Small*, 2018, **14**, 1801454.

33 H. V. Doan, H. Amer Hamzah, P. Karikkethu Prabhakaran, C. Petrillo and V. P. Ting, Hierarchical Metal-Organic Frameworks with Macroporosity: Synthesis, Achievements, and Challenges, *Nano-Micro Lett.*, 2019, **11**, 54.

34 L. Feng, K. Y. Wang, G. S. Day and H. C. Zhou, The chemistry of multi-component and hierarchical framework compounds, *Chem. Soc. Rev.*, 2019, **48**, 4823–4853.

35 Y. Luo, M. Ahmad, A. Schug and M. Tsotsalas, Rising Up: Hierarchical Metal-Organic Frameworks in Experiments and Simulations, *Adv. Mater.*, 2019, **31**, 1901744.

36 L. Feng, K.-Y. Wang, X.-L. Lv, T.-H. Yan and H.-C. Zhou, Hierarchically porous metal–organic frameworks: synthetic strategies and applications, *Natl. Sci. Rev.*, 2020, **7**, 1743–1758.

37 R. Haldar and C. Wöll, Hierarchical assemblies of molecular frameworks—MOF-on-MOF epitaxial heterostructures, *Nano Res.*, 2020, **14**, 355–368.

38 F. Lorignon, A. Gossard and M. Carboni, Hierarchically porous monolithic MOFs: An ongoing challenge for industrial-scale effluent treatment, *Chem. Eng. J.*, 2020, **393**, 124765.

39 N. Zhao, K. Cai and H. He, The synthesis of metal-organic frameworks with template strategies, *Dalton Trans.*, 2020, **49**, 11467–11479.

40 G. Cai, P. Yan, L. Zhang, H. C. Zhou and H. L. Jiang, Metal-Organic Framework-Based Hierarchically Porous Materials: Synthesis and Applications, *Chem. Rev.*, 2021, **121**, 12278–12326.

41 C. Duan, K. Liang, J. Lin, J. Li, L. Li, L. Kang, Y. Yu and H. Xi, Application of hierarchically porous metal-organic frameworks in heterogeneous catalysis: A review, *Sci. China Mater.*, 2021, **65**, 298–320.

42 C. Liu, J. Wang, J. Wan and C. Yu, MOF-on-MOF hybrids: Synthesis and applications, *Coord. Chem. Rev.*, 2021, **432**, 213743.

43 A. Saad, S. Biswas, E. Gkaniatsou, C. Sicard, E. Dumas, N. Menguy and N. Steunou, Metal–Organic Framework Based 1D Nanostructures and Their Superstructures: Synthesis, Microstructure, and Properties, *Chem. Mater.*, 2021, **33**, 5825–5849.

44 X. Zhang, R. Tu, Z. Lu, J. Peng, C. Hou and Z. Wang, Hierarchical mesoporous metal–organic frameworks encapsulated enzymes: Progress and perspective, *Coord. Chem. Rev.*, 2021, **443**, 214032.

45 X. Yin, A. Alsuwaidi and X. Zhang, Hierarchical metal–organic framework (MOF) pore engineering, *Microporous Mesoporous Mater.*, 2022, **330**, 111633.

46 T. M. Osborn Popp, A. Z. Plantz, O. M. Yaghi and J. A. Reimer, Precise Control of Molecular Self-Diffusion in Isoreticular and Multivariate Metal-Organic Frameworks, *Chem. Phys. Chem.*, 2020, **21**, 32–35.

47 S. J. D. Smith, B. P. Ladewig, A. J. Hill, C. H. Lau and M. R. Hill, Post-synthetic Ti Exchanged UiO-66 Metal-Organic Frameworks that Deliver Exceptional Gas Permeability in Mixed Matrix Membranes, *Sci. Rep.*, 2015, **5**, 7823.

48 C. H. Lau, R. Babarao and M. R. Hill, A route to drastic increase of CO_2 uptake in Zr metal organic framework UiO-66, *Chem. Commun.*, 2013, **49**, 3634–3636.

49 L. J. Wang, H. Deng, H. Furukawa, F. Gandara, K. E. Cordova, D. Peri and O. M. Yaghi, Synthesis and characterization of metal-organic framework-74 containing 2, 4, 6, 8, and 10 different metals, *Inorg. Chem.*, 2014, **53**, 5881–5883.

50 H. Deng, C. J. Doonan, H. Furukawa, R. B. Ferreira, J. Towne, C. B. Knobler, B. Wang and O. M. Yaghi, Multiple functional groups of varying ratios in metal-organic frameworks, *Science*, 2010, **327**, 846–850.

51 J. Jin, P. Li, D. H. Chun, B. Jin, K. Zhang and J. H. Park, Defect Dominated Hierarchical Ti-Metal–Organic Frameworks via a Linker Competitive Coordination Strategy for Toluene Removal, *Adv. Funct. Mater.*, 2021, **31**, 2102511.

52 O. Kozachuk, I. Luz, F. X. Llabrés i Xamena, H. Noei, M. Kauer, H. B. Albada, E. D. Bloch, B. Marler, Y. Wang, M. Muhler and R. A. Fischer, Multifunctional, Defect-Engineered Metal–Organic Frameworks with Ruthenium Centers: Sorption and Catalytic Properties, *Angew. Chem., Int. Ed.*, 2014, **53**, 7058–7062.

53 G. C. Shearer, J. G. Vitillo, S. Bordiga, S. Svelle, U. Olsbye and K. P. Lillerud, Functionalizing the Defects: Postsynthetic Ligand Exchange in the Metal Organic Framework UiO-66, *Chem. Mater.*, 2016, **28**, 7190–7193.

54 M. Taddei, R. J. Wakeham, A. Koutsianos, E. Andreoli and A. R. Barron, Post-Synthetic Ligand Exchange in Zirconium-Based Metal-Organic Frameworks: Beware of The Defects!, *Angew. Chem., Int. Ed.*, 2018, **57**, 11706–11710.

55 J. A. Boissonnault, A. G. Wong-Foy and A. J. Matzger, Core-Shell Structures Arise Naturally During Ligand Exchange in Metal-Organic Frameworks, *J. Am. Chem. Soc.*, 2017, **139**, 14841–14844.

56 M. Kim, J. F. Cahill, H. Fei, K. A. Prather and S. M. Cohen, Postsynthetic ligand and cation exchange in robust metal-organic frameworks, *J. Am. Chem. Soc.*, 2012, **134**, 18082–18088.

57 G. Cai, X. Ma, M. Kassymova, K. Sun, M. Ding and H. L. Jiang, Large-Scale Production of Hierarchically Porous Metal-Organic Frameworks by a Reflux-Assisted Post-Synthetic Ligand Substitution Strategy, *ACS Cent. Sci.*, 2021, **7**, 1434–1440.

58 S. Yuan, L. Zou, J. S. Qin, J. Li, L. Huang, L. Feng, X. Wang, M. Bosch, A. Alsalme, T. Cagin and H. C. Zhou, Construction of hierarchically porous metal-organic frameworks through linker labilization, *Nat. Commun.*, 2017, **8**, 15356.

59 L. Feng, S. Yuan, L. Zhang, K. Tan, J. Li, A. Kirchon, L. Liu, P. Zhang, Y. Han, Y. J. Chabal and H. Zhou, Creating Hierarchical Pores by Controlled Linker Thermolysis in Multivariate Metal-Organic Frameworks, *J. Am. Chem. Soc.*, 2018, **140**, 2363–2372.

60 P. Yang, F. Mao, Y. Li, Q. Zhuang and J. Gu, Hierarchical Porous Zr-Based MOFs Synthesized by a Facile Monocarboxylic Acid Etching Strategy, *Chemistry*, 2018, **24**, 2962–2970.

61 Y. Kim, T. Yang, G. Yun, M. B. Ghasemian, J. Koo, E. Lee, S. J. Cho and K. Kim, Hydrolytic Transformation of Microporous Metal-Organic Frameworks to Hierarchical Micro- and Mesoporous MOFs, *Angew. Chem., Int. Ed.*, 2015, **54**, 13273–13278.

62 S. C. Qi, X. Y. Qian, Q. X. He, K. J. Miao, Y. Jiang, P. Tan, X. Q. Liu and L. B. Sun, Generation of Hierarchical Porosity in Metal-Organic Frameworks by the Modulation of Cation Valence, *Angew. Chem., Int. Ed.*, 2019, **58**, 10104–10109.

63 D. Song, J. Bae, H. Ji, M.-B. Kim, Y.-S. Bae, K. S. Park, D. Moon and N. C. Jeong, Coordinative Reduction of Metal Nodes Enhances the Hydrolytic Stability of a Paddlewheel Metal–Organic Framework, *J. Am. Chem. Soc.*, 2019, **141**, 7853–7864.

64 L. Liu, Z. Chen, J. Wang, D. Zhang, Y. Zhu, S. Ling, K. W. Huang, Y. Belmabkhout, K. Adil, Y. Zhang, B. Slater, M. Eddaoudi and Y. Han, Imaging defects and their evolution in a metal-organic framework at sub-unit-cell resolution, *Nat. Chem.*, 2019, **11**, 622–628.

65 S.-Y. Kim, A.-R. Kim, J. W. Yoon, H.-J. Kim and Y.-S. Bae, Creation of mesoporous defects in a microporous metal-organic framework by an acetic acid-fragmented linker

co-assembly and its remarkable effects on methane uptake, *Chem. Eng. J.*, 2018, **335**, 94–100.

66 A. Kirchon, J. Li, F. Xia, G. S. Day, B. Becker, W. Chen, H. J. Sue, Y. Fang and H. C. Zhou, Modulation versus Templating: Fine-Tuning of Hierarchally Porous PCN-250 Using Fatty Acids To Engineer Guest Adsorption, *Angew. Chem., Int. Ed.*, 2019, **58**, 12425–12430.

67 G. Cai and H. L. Jiang, A Modulator-Induced Defect-Formation Strategy to Hierarchically Porous Metal-Organic Frameworks with High Stability, *Angew. Chem., Int. Ed.*, 2017, **56**, 563–567.

68 B. Liu, Y. Li, S. C. Oh, Y. Fang and H. Xi, Fabrication of a hierarchically structured HKUST-1 by a mixed-ligand approach, *RSC Adv.*, 2016, **6**, 61006–61012.

69 J. Wang, L. Liu, C. Chen, X. Dong, Q. Wang, L. Alfilfil, M. R. AlAlouni, K. Yao, J. Huang, D. Zhang and Y. Han, Engineering effective structural defects of metal–organic frameworks to enhance their catalytic performances, *J. Mater. Chem. A*, 2020, **8**, 4464–4472.

70 L. G. Qiu, T. Xu, Z. Q. Li, W. Wang, Y. Wu, X. Jiang, X. Y. Tian and L. D. Zhang, Hierarchically micro- and mesoporous metal-organic frameworks with tunable porosity, *Angew. Chem., Int. Ed.*, 2008, **47**, 9487–9491.

71 B. Seoane, A. Dikhtiarenko, A. Mayoral, C. Tellez, J. Coronas, F. Kapteijn and J. Gascon, Metal organic framework synthesis in the presence of surfactants: towards hierarchical MOFs?, *CrystEngComm*, 2015, **17**, 1693–1700.

72 L. B. Sun, J. R. Li, J. Park and H. C. Zhou, Cooperative template-directed assembly of mesoporous metal-organic frameworks, *J. Am. Chem. Soc.*, 2012, **134**, 126–129.

73 G. J. d A. A. Soler-Illia, C. Sanchez, B. Lebeau and J. Patarin, Chemical Strategies To Design Textured Materials: from Microporous and Mesoporous Oxides to Nanonetworks and Hierarchical Structures, *Chem. Rev.*, 2002, **102**, 4093–4138.

74 P. Rani and R. Srivastava, Exploring the dicationic gemini surfactant for the generation of mesopores: a step towards the construction of a hierarchical metal–organic framework, *Inorg. Chem. Front.*, 2018, **5**, 2856–2867.

75 X. Zhang, C. Y. Chuah, P. Dong, Y.-H. Cha, T.-H. Bae and M.-K. Song, Hierarchically Porous Co-MOF-74 Hollow Nanorods for Enhanced Dynamic CO_2 Separation, *ACS Appl. Mater. Interfaces*, 2018, **10**, 43316–43322.

76 X. Kang, K. Lyu, L. Li, J. Li, L. Kimberley, B. Wang, L. Liu, Y. Cheng, M. D. Frogley, S. Rudic, A. J. Ramirez-Cuesta, R. A. W. Dryfe, B. Han, S. Yang and M. Schroder, Integration of mesopores and crystal defects in metal-organic frameworks via templated electrosynthesis, *Nat. Commun.*, 2019, **10**, 4466.

77 L. Peng, J. Zhang, Z. Xue, B. Han, X. Sang, C. Liu and G. Yang, Highly mesoporous metal-organic framework assembled in a switchable solvent, *Nat. Commun.*, 2014, **5**, 4465.

78 Y. Yue, Z. A. Qiao, P. F. Fulvio, A. J. Binder, C. Tian, J. Chen, K. M. Nelson, X. Zhu and S. Dai, Template-free synthesis of hierarchical porous metal-organic frameworks, *J. Am. Chem. Soc.*, 2013, **135**, 9572–9575.

79 Y. Cao, Y. Ma, T. Wang, X. Wang, Q. Huo and Y. Liu, Facile Fabricating Hierarchically Porous Metal–Organic Frameworks via a Template-Free Strategy, *Cryst. Growth Des.*, 2015, **16**, 504–510.

80 J. X. Li, G. G. Chang, G. Tian, C. Pu, K. X. Huang, S. C. Ke, C. Janiak and X. Y. Yang, Near-Linear Controllable Synthesis of Mesoporosity in Hierarchical UiO-66 by Template-Free Nucleation-Competition, *Adv. Funct. Mater.*, 2021, **31**, 2102868.

81 S. Furukawa, K. Hirai, Y. Takashima, K. Nakagawa, M. Kondo, T. Tsuruoka, O. Sakata and S. Kitagawa, A block PCP crystal: anisotropic hybridization of porous coordination polymers by face-selective epitaxial growth, *Chem. Commun.*, 2009, 5097–5099.

82 M. Zhao, J. Chen, B. Chen, X. Zhang, Z. Shi, Z. Liu, Q. Ma, Y. Peng, C. Tan, X. J. Wu and H. Zhang, Selective Epitaxial Growth of Oriented Hierarchical Metal-Organic Framework Heterostructures, *J. Am. Chem. Soc.*, 2020, **142**, 8953–8961.

83 J. Zhuang, L. Y. Chou, B. T. Sneed, Y. Cao, P. Hu, L. Feng and C. K. Tsung, Surfactant-Mediated Conformal Overgrowth of Core-Shell Metal-Organic Framework Materials with Mismatched Topologies, *Small*, 2015, **11**, 5551–5555.

84 K.-Y. Wang, L. Feng, T.-H. Yan, J.-S. Qin, C.-X. Li and H.-C. Zhou, Morphology Transcription in Hierarchical MOF-on-MOF Architectures, *ACS Materials Lett.*, 2021, **3**, 738–743.

85 Q. Zha, M. Li, Z. Liu and Y. Ni, Hierarchical Co,Fe-MOF-74/ Co/Carbon Cloth Hybrid Electrode: Simple Construction and Enhanced Catalytic Performance in Full Water Splitting, *ACS Sustainable Chem. Eng.*, 2020, **8**, 12025–12035.

86 K. A. McDonald, J. I. Feldblyum, K. Koh, A. G. Wong-Foy and A. J. Matzger, Polymer@MOF@MOF: "grafting from" atom transfer radical polymerization for the synthesis of hybrid porous solids, *Chem. Commun.*, 2015, **51**, 11994–11996.

87 J. Ren, N. M. Musyoka, H. W. Langmi, B. C. North, M. Mathe and X. Kang, Fabrication of core–shell MIL-101(Cr)@UiO-66(Zr) nanocrystals for hydrogen storage, *Int. J. Hydrogen Energy*, 2014, **39**, 14912–14917.

88 X. Yang, S. Yuan, L. Zou, H. Drake, Y. Zhang, J. Qin, A. Alsalme and H. C. Zhou, One-Step Synthesis of Hybrid Core-Shell Metal-Organic Frameworks, *Angew. Chem., Int. Ed.*, 2018, **57**, 3927–3932.

89 M. R. Lohe, M. Rose and S. Kaskel, Metal-organic framework (MOF) aerogels with high micro- and macroporosity, *Chem. Commun.*, 2009, 6056–6058.

90 S. Xiang, L. Li, J. Zhang, X. Tan, H. Cui, J. Shi, Y. Hu, L. Chen, C.-Y. Su and S. L. James, Porous organic–inorganic hybrid aerogels based on Cr^{3+}/Fe^{3+} and rigid bridging carboxylates, *J. Mater. Chem.*, 2012, **22**, 1862–1867.

91 S. Głowniak, B. Szczęśniak, J. Choma and M. Jaroniec, Mechanochemistry: Toward green synthesis of metal–organic frameworks, *Mater. Today*, 2021, **46**, 109–124.

92 D. Lv, Y. Chen, Y. Li, R. Shi, H. Wu, X. Sun, J. Xiao, H. Xi, Q. Xia and Z. Li, Efficient Mechanochemical Synthesis of

MOF-5 for Linear Alkanes Adsorption, *J. Chem. Eng. Data*, 2017, **62**, 2030–2036.

93 X. Sun, H. Li, Y. Li, F. Xu, J. Xiao, Q. Xia, Y. Li and Z. Li, A novel mechanochemical method for reconstructing the moisture-degraded HKUST-1, *Chem. Commun.*, 2015, **51**, 10835–10838.

94 K. Leng, Y. Sun, X. Li, S. Sun and W. Xu, Rapid Synthesis of Metal–Organic Frameworks MIL-101(Cr) Without the Addition of Solvent and Hydrofluoric Acid, *Cryst. Growth Des.*, 2016, **16**, 1168–1171.

95 L. S. Germann, A. D. Katsenis, I. Huskić, P. A. Julien, K. Užarević, M. Etter, O. K. Farha, T. Friščić and R. E. Dinnebier, Real-Time in Situ Monitoring of Particle and Structure Evolution in the Mechanochemical Synthesis of UiO-66 Metal–Organic Frameworks, *Cryst. Growth Des.*, 2020, **20**, 49–54.

96 T. D. Bennett, S. Cao, J. C. Tan, D. A. Keen, E. G. Bithell, P. J. Beldon, T. Friscic and A. K. Cheetham, Facile mechanosynthesis of amorphous zeolitic imidazolate frameworks, *J. Am. Chem. Soc.*, 2011, **133**, 14546–14549.

97 M. Taheri, I. D. Bernardo, A. Lowe, D. R. Nisbet and T. Tsuzuki, Green Full Conversion of ZnO Nanopowders to Well-Dispersed Zeolitic Imidazolate Framework-8 (ZIF-8) Nanopowders via a Stoichiometric Mechanochemical Reaction for Fast Dye Adsorption, *Cryst. Growth Des.*, 2020, **20**, 2761–2773.

98 M. Rubio-Martinez, C. Avci-Camur, A. W. Thornton, I. Imaz, D. Maspoch and M. R. Hill, New synthetic routes towards MOF production at scale, *Chem. Soc. Rev.*, 2017, **46**, 3453–3480.

99 J. Yang, X. Feng, G. Lu, Y. Li, C. Mao, Z. Wen and W. Yuan, NaCl as a solid solvent to assist the mechanochemical synthesis and post-synthesis of hierarchical porous MOFs with high I_2 vapour uptake, *Dalton Trans.*, 2018, **47**, 5065–5071.

100 S. Tanaka, T. Nagaoka, A. Yasuyoshi, Y. Hasegawa and J. F. M. Denayer, Hierarchical Pore Development of ZIF-8 MOF by Simple Salt-Assisted Mechanosynthesis, *Cryst. Growth Des.*, 2017, **18**, 274–279.

101 P. A. Julien, K. Uzarevic, A. D. Katsenis, S. A. Kimber, T. Wang, O. K. Farha, Y. Zhang, J. Casaban, L. S. Germann, M. Etter, R. E. Dinnebier, S. L. James, I. Halasz and T. Friscic, In Situ Monitoring and Mechanism of the Mechanochemical Formation of a Microporous MOF-74 Framework, *J. Am. Chem. Soc.*, 2016, **138**, 2929–2932.

102 D. Tan and F. García, Main group mechanochemistry: from curiosity to established protocols, *Chem. Soc. Rev.*, 2019, **48**, 2274–2292.

103 A. J. Howarth, Y. Liu, P. Li, Z. Li, T. C. Wang, J. T. Hupp and O. K. Farha, Chemical, thermal and mechanical stabilities of metal–organic frameworks, *Nat. Rev. Mater.*, 2016, **1**, 15018.

104 A. R. Abbasi, M. Rizvandi, A. Azadbakht and S. Rostamnia, Controlled uptake and release of imatinib from ultrasound nanoparticles $Cu_3(BTC)_2$ metal-organic framework in comparison with bulk structure, *J. Colloid Interface Sci.*, 2016, **471**, 112–117.

105 A. R. Abbasi, M. Karimi and K. Daasbjerg, Efficient removal of crystal violet and methylene blue from wastewater by ultrasound nanoparticles Cu-MOF in comparison with mechanosynthesis method, *Ultrason. Sonochem.*, 2017, **37**, 182–191.

106 H. Thakkar, S. Eastman, Q. Al-Naddaf, A. A. Rownaghi and F. Rezaei, 3D-Printed Metal-Organic Framework Monoliths for Gas Adsorption Processes, *ACS Appl. Mater. Interfaces*, 2017, **9**, 35908–35916.

107 E. R. Kearns, R. Gillespie and D. M. D'Alessandro, 3D printing of metal–organic framework composite materials for clean energy and environmental applications, *J. Mater. Chem. A*, 2021, **9**, 27252–27270.

108 S. Lawson, A.-A. Alwakwak, A. A. Rownaghi and F. Rezaei, Gel–Print–Grow: A New Way of 3D Printing Metal–Organic Frameworks, *ACS Appl. Mater. Interfaces*, 2020, **12**, 56108–56117.

109 A. Figuerola, D. A. V. Medina, A. J. Santos-Neto, C. P. Cabello, V. Cerdà, G. T. Palomino and F. Maya, Metal–organic framework mixed-matrix coatings on 3D printed devices, *Appl. Mater. Today*, 2019, **16**, 21–27.

110 S. Sultan, H. N. Abdelhamid, X. Zou and A. P. Mathew, CelloMOF: Nanocellulose Enabled 3D Printing of Metal-Organic Frameworks, *Adv. Funct. Mater.*, 2019, **29**, 1805372.

111 R. Semino, J. C. Moreton, N. A. Ramsahye, S. M. Cohen and G. Maurin, Understanding the origins of metal-organic framework/polymer compatibility, *Chem. Sci.*, 2018, **9**, 315–324.

112 M. N. Channell, M. Sefa, J. A. Fedchak, J. Scherschligt, M. Bible, B. Natarajan, N. N. Klimov, A. E. Miller, Z. Ahmed and M. R. Hartings, Toward 3D Printed Hydrogen Storage Materials Made with ABS-MOF Composites, *Polym. Adv. Technol.*, 2018, **29**, 867–873.

113 H. Li, K. Wang, Y. Sun, C. T. Lollar, J. Li and H.-C. Zhou, Recent advances in gas storage and separation using metal–organic frameworks, *Mater. Today*, 2018, **21**, 108–121.

114 M. Ding, R. W. Flaig, H. L. Jiang and O. M. Yaghi, Carbon capture and conversion using metal-organic frameworks and MOF-based materials, *Chem. Soc. Rev.*, 2019, **48**, 2783–2828.

115 Y. Wang, X. Jia, H. Yang, Y. Wang, X. Chen, A. N. Hong, J. Li, X. Bu and P. Feng, A Strategy for Constructing Pore-Space-Partitioned MOFs with High Uptake Capacity for C_2 Hydrocarbons and CO_2, *Angew. Chem., Int. Ed.*, 2020, **59**, 19027–19030.

116 S. Ghosh, A. Modak, A. Samanta, K. Kole and S. Jana, Recent progress in materials development for CO_2 conversion: issues and challenges, *Mater. Adv.*, 2021, **2**, 3161–3187.

117 T. Ghanbari, F. Abnisa and W. M. A. Wan, Daud, A review on production of metal organic frameworks (MOF) for CO_2 adsorption, *Sci. Total Environ.*, 2020, **707**, 135090.

118 C. C. Liang, Z. L. Shi, C. T. He, J. Tan, H. D. Zhou, H. L. Zhou, Y. Lee and Y. B. Zhang, Engineering of Pore Geometry for Ultrahigh Capacity Methane Storage in

Mesoporous Metal-Organic Frameworks, *J. Am. Chem. Soc.*, 2017, **139**, 13300–13303.

119 X. Yin and X. Zhang, Hierarchical metal–organic frameworks constructed from intergrowth for the adsorption of light hydrocarbons, *Mater. Chem. Front.*, 2020, **4**, 3057–3062.

120 G. J. H. Lim, Y. Wu, B. B. Shah, J. J. Koh, C. K. Liu, D. Zhao, A. K. Cheetham, J. Wang and J. Ding, 3D-Printing of Pure Metal–Organic Framework Monoliths, *ACS Mater. Lett.*, 2019, **1**, 147–153.

121 X. Zhang, S. Zheng, J. Tao and X. Wang, In Situ Encapsulation of Cellulase in a Novel Mesoporous Metal–Organic Framework, *Catal. Lett.*, 2021, **152**, 699–706.

122 S. E. Bambalaza, H. W. Langmi, R. Mokaya, N. M. Musyoka and L. E. Khotseng, Co-pelletization of a zirconium-based metal-organic framework (UiO-66) with polymer nanofibers for improved useable capacity in hydrogen storage, *Int. J. Hydrogen Energy*, 2021, **46**, 8607–8620.

123 X.-X. Huang, L.-G. Qiu, W. Zhang, Y.-P. Yuan, X. Jiang, A.-J. Xie, Y.-H. Shen and J.-F. Zhu, Hierarchically mesostructured MIL-101 metal–organic frameworks: supramolecular template-directed synthesis and accelerated adsorption kinetics for dye removal, *CrystEngComm*, 2012, **14**, 1613–1617.

124 H. N. Abdelhamid and X. Zou, Template-free and room temperature synthesis of hierarchical porous zeolitic imidazolate framework nanoparticles and their dye and CO_2 sorption, *Green Chem.*, 2018, **20**, 1074–1084.

125 J. Park, Z. U. Wang, L. B. Sun, Y. P. Chen and H. C. Zhou, Introduction of functionalized mesopores to metal-organic frameworks via metal-ligand-fragment coassembly, *J. Am. Chem. Soc.*, 2012, **134**, 20110–20116.

126 W. Wu, J. Su, M. Jia, Z. Li, G. Liu and W. Li, Vapor-phase linker exchange of metal-organic frameworks, *Sci. Adv.*, 2020, **6**, eaax7270.

127 Y. Mao, D. Chen, P. Hu, Y. Guo, Y. Ying, W. Ying and X. Peng, Hierarchical Mesoporous Metal-Organic Frameworks for Enhanced CO_2 Capture, *Chemistry*, 2015, **21**, 15127–15132.

128 H. Zhang, C. Duan, F. Li, X. Yan and H. Xi, Green and rapid synthesis of hierarchical porous zeolitic imidazolate frameworks for enhanced CO_2 capture, *Inorg. Chim. Acta*, 2018, **482**, 358–363.

129 Z. Li, X. Xing, D. Meng, Z. Wang, J. Xue, R. Wang, J. Chu, M. Li and Y. Yang, Hierarchical Structure with Highly Ordered Macroporous-Mesoporous Metal-Organic Frameworks as Dual Function for CO2 Fixation, *iScience*, 2019, **15**, 514–523.

130 C. Wang, X. Liu, W. Li, X. Huang, S. Luan, X. Hou, M. Zhang and Q. Wang, CO_2 mediated fabrication of hierarchically porous metal-organic frameworks, *Microporous Mesoporous Mater.*, 2019, **277**, 154–162.

131 C. Zhou, L. Cao, S. Wei, Q. Zhang and L. Chen, A first principles study of gas adsorption on charged CuBTC, *Comput. Theor. Chem.*, 2011, **976**, 153–160.

132 T. Li, J. E. Sullivan and N. L. Rosi, Design and preparation of a core-shell metal-organic framework for selective CO_2 capture, *J. Am. Chem. Soc.*, 2013, **135**, 9984–9987.

133 D. K. Panchariya, R. K. Rai, E. Anil Kumar and S. K. Singh, Core-Shell Zeolitic Imidazolate Frameworks for Enhanced Hydrogen Storage, *ACS Omega*, 2018, **3**, 167–175.

134 D. Kim, D. W. Kim, W. G. Hong and A. Coskun, Graphene/ZIF-8 composites with tunable hierarchical porosity and electrical conductivity, *J. Mater. Chem. A*, 2016, **4**, 7710–7717.

135 D. Wisser, F. M. Wisser, S. Raschke, N. Klein, M. Leistner, J. Grothe, E. Brunner and S. Kaskel, Biological Chitin-MOF Composites with Hierarchical Pore Systems for Air-Filtration Applications, *Angew. Chem., Int. Ed.*, 2015, **54**, 12588–12591.

136 Y. Zhang, S. Yuan, X. Feng, H. Li, J. Zhou and B. Wang, Preparation of Nanofibrous Metal-Organic Framework Filters for Efficient Air Pollution Control, *J. Am. Chem. Soc.*, 2016, **138**, 5785–5788.

137 N. A. Khan, Z. Hasan and S. H. Jhung, Adsorptive removal of hazardous materials using metal-organic frameworks (MOFs): a review, *J. Hazard. Mater.*, 2013, **244–245**, 444–456.

138 Y. Chen, S. Zhang, S. Cao, S. Li, F. Chen, S. Yuan, C. Xu, J. Zhou, X. Feng, X. Ma and B. Wang, Roll-to-Roll Production of Metal-Organic Framework Coatings for Particulate Matter Removal, *Adv. Mater.*, 2017, **29**, 1606221.

139 B.-J. Zhu, X.-Y. Yu, Y. Jia, F.-M. Peng, B. Sun, M.-Y. Zhang, T. Luo, J.-H. Liu and X.-J. Huang, Iron and 1,3,5-Benzenetricarboxylic Metal–Organic Coordination Polymers Prepared by Solvothermal Method and Their Application in Efficient As(V) Removal from Aqueous Solutions, *J. Phys. Chem. C*, 2012, **116**, 8601–8607.

140 J. Jiang, R. Babarao and Z. Hu, Molecular simulations for energy, environmental and pharmaceutical applications of nanoporous materials: from zeolites, metal-organic frameworks to protein crystals, *Chem. Soc. Rev.*, 2011, **40**, 3599–3612.

141 J. Cai, X. Wang, Y. Zhou, L. Jiang and C. Wang, Selective adsorption of arsenate and the reversible structure transformation of the mesoporous metal-organic framework MIL-100(Fe), *Phys. Chem. Chem. Phys.*, 2016, **18**, 10864–10867.

142 C. Wang, X. Liu, J. P. Chen and K. Li, Superior removal of arsenic from water with zirconium metal-organic framework UiO-66, *Sci. Rep.*, 2015, **5**, 16613.

143 J. Wen, P. He, C. Lei, E. Lv, Y. Wu, J. Gao and J. Yao, Fabrication of metal-organic framework@Yeast composite materials for efficient removal of Pb2+ in water, *J. Solid State Chem.*, 2019, **274**, 26–31.

144 Y. N. Wu, M. Zhou, B. Zhang, B. Wu, J. Li, J. Qiao, X. Guan and F. Li, Amino acid assisted templating synthesis of hierarchical zeolitic imidazolate framework-8 for efficient arsenate removal, *Nanoscale*, 2014, **6**, 1105–1112.

145 D. Mutruc, A. Goulet-Hanssens, S. Fairman, S. Wahl, A. Zimathies, C. Knie and S. Hecht, Modulating Guest Uptake in Core-Shell MOFs with Visible Light, *Angew. Chem., Int. Ed.*, 2019, **58**, 12862–12867.

146 P. Li, J. A. Modica, A. J. Howarth, E. Vargas, L. Peyman, Z. Moghadam, R. Q. Snurr, M. Mrksich, J. T. Hupp and O. K. Farha, Toward Design Rules for Enzyme

Immobilization in Hierarchical Mesoporous Metal-Organic Frameworks, *Chem*, 2016, **1**, 154–169.

147 J. Cui, N. Gao, X. Yin, W. Zhang, Y. Liang, L. Tian, K. Zhou, S. Wang and G. Li, Microfluidic synthesis of uniform single-crystalline MOF microcubes with a hierarchical porous structure, *Nanoscale*, 2018, **10**, 9192–9198.

148 W. Zhang, Y. Liu, G. Lu, Y. Wang, S. Li, C. Cui, J. Wu, Z. Xu, D. Tian, W. Huang, J. S. DuCheneu, W. D. Wei, H. Chen, Y. Yang and F. Huo, Mesoporous metal-organic frameworks with size-, shape-, and space-distribution-controlled pore structure, *Adv. Mater.*, 2015, **27**, 2923–2929.

149 X. Zhai and Y. Fu, Preparation of Hierarchically Porous Metal–Organic Frameworks via Slow Chemical Vapor Etching for CO_2 Cycloaddition, *Inorg. Chem.*, 2022, **61**, 6881–6887.

150 H. F. Drake, Z. Xiao, G. S. Day, S. W. Vali, W. Chen, Q. Wang, Y. Huang, T.-H. Yan, J. E. Kuszynski, P. A. Lindahl, M. R. Ryder and H.-C. Zhou, Thermal decarboxylation for the generation of hierarchical porosity in isostructural metal–organic frameworks containing open metal sites, *Mater. Adv.*, 2021, **2**, 5487–5493.

151 M. K. Dinker, K. Zhao, X.-Q. Liu and L.-B. Sun, Solitary Medium of a Multifunctional Ionic Liquid for Crystallizing Hierarchically Porous Metal–Organic Frameworks, *Inorg. Chem.*, 2022, **61**, 10393–10401.

152 K.-Y. Wang, L. Feng, T.-H. Yan, S. Wu, E. A. Joseph and H.-C. Zhou, Rapid Generation of Hierarchically Porous Metal–Organic Frameworks through Laser Photolysis, *Angew. Chem., Int. Ed.*, 2020, **59**, 11349–11354.